Cellular & Molecular Immunology www.nature.com/cmi

ARTICLE

CD147 regulates antitumor CD8$^+$ T-cell responses to facilitate tumor-immune escape

Yatong Chen[1], Jing Xu[1,2], Xiaodong Wu[1,3], Hui Yao[1,4], Zhou Yan[1], Ting Guo[1], Wenjing Wang[1], Peixiao Wang[1,5], Yu Li[1], Xiangmin Yang[1], Hao Li[1], Huijie Bian[1] and Zhi-Nan Chen[1]

Negative regulation of antitumor T-cell-immune responses facilitates tumor-immune escape. Here, we show that deletion of CD147, a type I transmembrane molecule, in T cells, strongly limits in vivo tumor growth of mouse melanoma and lung cancer in a CD8$^+$ T-cell-dependent manner. In mouse tumor models, CD147 expression was upregulated on CD8$^+$ tumor-infiltrating lymphocytes (TILs), and CD147 was coexpressed with two immune-checkpoint molecules, Tim-3 and PD-1. Mining publicly available gene-profiling data for CD8$^+$ TILs in tumor biopsies from metastatic melanoma patients showed a higher level of CD147 expression in exhausted CD8$^+$ TILs than in other subsets of CD8$^+$ TILs, along with expression of PD-1 and TIM-3. Additionally, CD147 deletion increased the abundance of TILs, cytotoxic effector function of CD8$^+$ T cells, and frequency of PD-1$^+$ CD8$^+$ TILs, and partly reversed the dysfunctional status of PD-1$^+$Tim-3$^+$CD8$^+$ TILs. The cytotoxic transcription factors Runx3 and T-bet mediation enhanced antitumor responses by CD147$^{-/-}$ CD8$^+$ T cells. Moreover, CD147 deletion in T cells increased the frequency of T_{RM}-like cells and the expression of the T-cell chemokines CXCL9 and CXCL10 in the tumor microenvironment. Analysis of tumor tissue samples from patients with non-small-cell lung cancer showed negative correlations between CD147 expression on CD8$^+$ TILs and the abundance of CD8$^+$ TILs, histological grade of the tumor tissue samples, and survival of patients with advanced tumors. Altogether, we found a novel function of CD147 as a negative regulator of antitumor responses mediated by CD8$^+$ TILs and identified CD147 as a potential target for cancer immunotherapy.

Keywords: CD147; CD8$^+$ T cells; Anti-tumor immunity

Cellular & Molecular Immunology (2021) 18:1995–2009; https://doi.org/10.1038/s41423-020-00570-y

INTRODUCTION

The presence of CD8$^+$ tumor-infiltrating lymphocytes (TILs) is believed to be an indicator of antitumor -immune responses to tumor antigens[1]; however, successful elimination of cancer cells by these TILs is hampered by a broad set of immunosuppressive mechanisms.[2] The coexistence of progressively growing tumors and CD8$^+$ TILs suggests that these TILs have a dysfunctional status upon chronic exposure to antigens[3] and an inhibitory tumor microenvironment (TME),[4,5] which is characterized by loss of the capacities to proliferate, produce cytotoxic cytokines, and lyse cancer cells.[2] Altered transcriptional and epigenetic programs have been found in dysfunctional CD8$^+$ TILs,[6] and these programs lead to increased expression of inhibitory receptors,[2] such as CTLA-4, PD-1, Tim-3, and LAG-3, to impede T-cell survival and functions and facilitate tumor-immune escape.[7–9] In recent years, the successful reinvigoration of T-cell function by antibodies targeting inhibitory receptors has resulted in robust and durable antitumor responses in different types of cancers, such as advanced melanoma, non-small-cell lung cancer (NSCLC), head and neck cancer, and kidney cancer.[10–12] However, most patients still exhibit primary or acquired resistance to immunotherapy, which is due to either cancer immunoediting[13] or the nonredundant suppressive effects of distinct inhibitory receptors,[14,15] emphasizing the need to understand additional mechanisms driving T-cell dysfunction, and identify new inhibitory molecules with the potential to be targeted to achieve functional rescue of CD8$^+$ TILs.

CD147 (also known as basigin, M6, and EMMPRIN), a transmembrane glycoprotein belonging to the immunoglobulin superfamily (IgSF), was originally identified as a T-cell activation-associated antigen[16] and a cancer-associated antigen,[17] as the expression of CD147 was found to be significantly upregulated in activated T cells and cancer cells. CD147 was also shown to be a surrogate marker for activated immunosuppressive regulatory T cells.[18,19] CD147 can regulate thymocyte maturation[20] and the migration,[21–23] invasion,[24,25] adhesion,[26,27] and aggregation[28] of T cells or T-lymphoma cells in some in vitro analyses or in murine models of inflammation in vivo. Antibodies specific to the extracellular domain of CD147 can trigger the dissociation of certain molecules from microdomains to shut down T-cell

[1]National Translational Science Center for Molecular Medicine & Department of Cell Biology, Fourth Military Medical University, 710032 Xi'an, China; [2]Medical Research Center, Southern University of Science and Technology Hospital, 518055 Shenzhen, China; [3]Center of Anesthesiology & Operation, Chinese PLA General Hospital, 100853 Beijing, China; [4]Department of Radiation Oncology, First Peoples' Hospital of Changzhou, Third Affiliated Hospital of Soochow University, 213000 Changzhou, China and [5]Department of Gastroenterology, Henan Children's Hospital, 450018 Zhengzhou, China
Correspondence: Jing Xu (lightxj@126.com) or Huijie Bian (hjbian@fmmu.edu.cn) or Zhi-Nan Chen (znchen@fmmu.edu.cn)
These authors contributed equally: Yatong Chen, Jing Xu, Xiaodong Wu

Received: 14 May 2020 Accepted: 9 October 2020
Published online: 11 November 2020

responses upon TCR-dependent activation of PBMCs.[29,30] In leukemic Jurkat T cells, transcriptional silencing of CD147 can enhance NF–AT transcriptional activity via JNK and p21-activated kinase 1.[31] CD147 was also reported to form a complex with plasma membrane calcium ATPase isoform 4 (PMCA4) to dampen IL-2 production via NFAT and NF-κB in leukemic Jurkat T cells and primary $CD4^+$ T cells.[32] In our previous study, we generated T-cell-specific *basigin* (CD147-encoding gene)-knockout mice (Lck–Cre; $Bsg^{flox/flox}$, recorded as $Bsg^{\Delta T}$) and found that $CD147^{-/-}$ $CD4^+$ T cells exhibited increased in vitro proliferation compared with $CD147^{+/+}$ $CD4^+$ T cells upon TCR-dependent activation.[33] These findings indicate that CD147 may play an inhibitory role in some T-cell responses, but the function of CD147 in $CD8^+$ T cells, especially in antitumor immunity, has not been established.

In this study, we found that the expression of CD147 on $CD8^+$ TILs was significantly upregulated in the TME, and that CD147 was coexpressed with PD-1 and Tim-3. T-cell-specific gene knockout of CD147 profoundly suppressed the in vivo growth of syngeneic mouse tumors in a $CD8^+$ T-cell-dependent manner and enhanced the abundance and cytotoxic activity of $CD8^+$ TILs, even that of $PD\text{-}1^+Tim\text{-}3^+$ $CD8^+$ TILs. Runx3 and T-bet might mediate the enhanced cytotoxic activity established by CD147 gene deletion. Moreover, the expression of CD147 on $CD8^+$ TILs was found to be negatively correlated with the abundance of $CD8^+$ TILs, histological grade, and survival of patients with NSCLC. Altogether, our results suggest that elevated expression of CD147 on $CD8^+$ TILs in the TME negatively regulates antitumor-immune responses and facilitates tumor-immune escape, which supports the conclusion that CD147 may be a potential candidate target for cancer immunotherapy.

RESULTS

CD147 expression is upregulated on $CD8^+$ TILs and strongly correlated with inhibitory receptor expression

To determine the expression patterns of CD147 in immune-cell subsets in the TME, we established a syngeneic Lewis lung cancer mouse model and measured the expression of CD147 on tumor-infiltrating and splenic $CD8^+$ T cells, $CD4^+$ T cells, and myeloid-derived suppressor cells (MDSCs) by flow-cytometry analysis. The results showed that the percentages of splenic $CD147^+CD8^+$ T cells, $CD147^+CD4^+$ T cells, and $CD147^+$ MDSCs were all increased in tumor-bearing mice compared to their tumor-free counterparts (Fig. 1A), suggesting that the tumor burden induced the expression of CD147 on splenic T cells and MDSCs. When comparing the expression of CD147 on tumor-infiltrating $CD8^+$ T cells, $CD4^+$ T cells, and MDSCs with that on the corresponding splenic cell subsets in the same individual mouse, a substantial increase in the $CD147^+$ subset of $CD8^+$ TILs was found, while no significant differences were found for $CD4^+$ T cells or MDSCs (Fig. 1B). These results suggest that upon upregulation by the tumor burden, the expression of CD147 on $CD8^+$ T cells is further upregulated in the TME and may play an indispensable role in tumor immunomodulation.

Then, we assessed the coexpression patterns of the inhibitory receptors PD-1 and Tim-3, the differentiation markers CD44 and CD103, and the chemokine receptor CXCR3 with CD147 on $CD8^+$ TILs. $CD8^+$ TILs displayed coexpression of Tim-3, PD-1, and CD44 with CD147. Tim-3 and PD-1 were almost exclusively expressed on $CD147^+$ cells: 75.3% ± 5.4% of $Tim\text{-}3^+CD8^+$ TILs and 70.1% ± 5.1% of $PD\text{-}1^+CD8^+$ TILs expressed CD147 in freshly isolated tumor tissue samples (Fig. 1C). However, CD44, CD103, and CXCR3 were not exclusively expressed on $CD147^+$ $CD8^+$ TILs, as there were still substantial percentages of $CD44^{high}$, $CD103^+$, and $CXCR3^+$ $CD8^+$ TILs that were $CD147^-$. On average, 55.6% ± 3.8% of $CD44^{high}$ $CD8^+$ TILs, 33.4% of $CD103^+$ $CD8^+$ TILs, and 26.2% of $CXCR3^+$ $CD8^+$ TILs expressed CD147 in the tumor tissue samples (Fig. 1C). Thus, the coexpression patterns of CD147 with PD-1 and Tim-3 appeared to be different from those of CD147 with CD44, CD103, and CXCR3, suggesting that CD147 may exert similar functions with the inhibitory receptors Tim-3 and PD-1 in $CD8^+$ TILs.

Furthermore, we performed data mining of publicly available scRNA-seq gene expression profiles of $CD8^+$ TILs isolated from tumor biopsies taken from metastatic melanoma patients in a previous study, in which $CD8^+$ TILs were classified into two subsets: CD8_G (analogous to a previously defined progenitor-exhausted $CD8^+$ T-cell subset in B16-OVA tumors[34]) with increased expression of genes linked to memory, activation, and cell survival and reduced expression of coinhibitory molecules, and CD8_B (analogous to a previously defined terminally exhausted $CD8^+$ T-cell subset in B16-OVA tumors[34]) enriched for genes linked to cell exhaustion.[35] Mining of the scRNA-seq data showed higher levels of *Bsg* (encoding CD147) ($P < 0.001$), *PDCD1* (encoding PD-1), and *HAVCR2* (encoding Tim-3) in the CD8_B subset than in the CD8_G subset (Fig. 1D). In six further subclusters, the CD8_1 subcluster (expressing markers similar to those of terminally exhausted $CD8^+$ T cells and being enriched in checkpoint therapy nonresponder lesions) had a higher expression level of Bsg transcripts than the other five subclusters ($P < 0.001$) (Fig. 1D). These results indicate that CD147 may be a negative regulator of $CD8^+$ TILs.

CD147 gene deletion in T cells inhibits tumor growth and enhances antitumor-immune responses

To study the functional roles of CD147 in TILs, we employed our previously constructed T-cell-specific CD147-knockout mice to establish syngeneic tumor models with melanoma B16–F10 cells and Lewis lung cancer (LLC) cells. For both B16 melanoma (Fig. 2A) and LLC (Fig. 2B), tumor formation and growth were dramatically inhibited, and tumor weight was significantly reduced in $Bsg^{\triangle T}$ (Lck–Cre; $Bsg^{flox/flox}$) mice compared to Bsg^{WT} ($Bsg^{flox/flox}$) littermates from the same breeding colonies, with tumor-inhibition rates of 87.71% for B16 melanoma and 57.74% for LLC, suggesting that T-cell-expressed CD147 may exert a tumor-promoting function in the TME.

To understand the immune mechanism underlying tumor inhibition by CD147 deficiency in T cells, we compared the immune phenotype between LLC or B16–F10 tumor-bearing $Bsg^{\triangle T}$ and Bsg^{WT} mice. In line with our previous finding that CD147 deficiency did not affect the activation state of unstimulated $CD4^+$ T cells,[33] no significant differences in CD69 or CD25 expression on peripheral $CD8^+$ T cells were found between $Bsg^{\triangle T}$ and Bsg^{WT} mice without tumor inoculation (Supplementary Fig. S1a), indicating that no significant difference in the activation state was caused by CD147 deficiency before tumor inoculation. Flow-cytometry analysis showed that the percentages of both $CD8^+$ TILs and $CD4^+$ TILs were dramatically increased in LLC tumor-bearing $Bsg^{\triangle T}$ mice compared to LLC tumor-bearing Bsg^{WT} mice (Fig. 2C), while no differences in splenic cells were observed between $Bsg^{\triangle T}$ and Bsg^{WT} mice (Fig. 2D). Additionally, the proportions of both tumor-infiltrating and splenic MDSCs were decreased in $Bsg^{\triangle T}$ mice compared to Bsg^{WT} mice (Fig. 2C, D). A similar tendency was also found in B16–F10 tumor-bearing mice by flow-cytometry analysis (Supplementary Fig. S1b, c) and immunofluorescence staining (Fig. 2E). These results suggested that the effective tumor control in $Bsg^{\triangle T}$ mice might be due to the enhanced antitumor immunity induced by T-cell CD147 deficiency.

CD147 deficiency augments the effector function of $CD8^+$ T cells

We used Lck–Cre to mediate pan-T-cell gene deletion and examined angiogenesis, cell proliferation, and apoptosis in B16–F10 melanoma tumor tissue samples. Immunofluorescence staining for CD31 and Ki67 showed that CD147 deficiency in T cells had no effects on angiogenesis or tumor cell proliferation (Fig. 3A). However, TUNEL analysis showed an increased

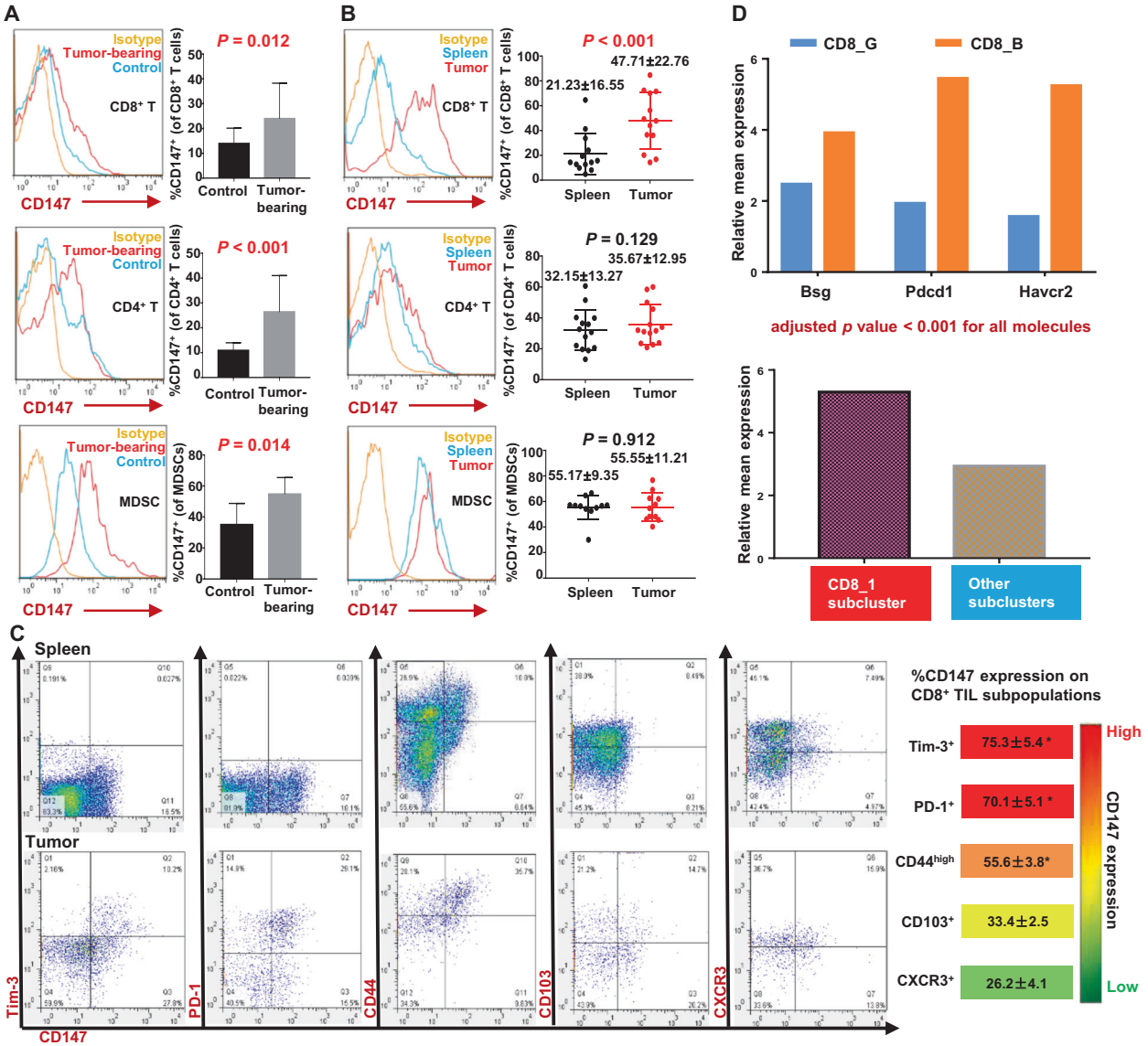

Fig. 1 CD147 expression is upregulated on $CD8^+$ TILs, and CD147 is coexpressed with the inhibitory receptors PD-1 and Tim-3. **A** Representative figures and summary data for CD147 expression on splenic $CD8^+$ T cells, $CD4^+$ T cells, and MDSCs from tumor-bearing or control mice. LLC cells (1×10^6/mouse) were s.c. inoculated into C57BL/6 mice (11–13 mice per group), while an equal volume of serum-free medium was s.c. injected into the mice in the control group (6–7 mice per group). Splenocytes were analyzed with flow cytometry on day 16 after inoculation. MDSCs were double-labeled with an anti-CD11b antibody and anti-Gr1 antibody (RB6-8C5, reacting with a common epitope in Ly-6G and Ly-6C). An isotype antibody was used as a negative control. **B** CD147 expression on tumor-infiltrating or splenic $CD8^+$ T cells, $CD4^+$ T cells, and MDSCs from LLC tumor-bearing mice (11–14 mice per group) was analyzed with flow cytometry on day 16 after inoculation. **C** Coexpression patterns of CD147 with Tim-3, PD-1, CD44, CD103, or CXCR3 on tumor-infiltrating and splenic $CD8^+$ T cells. B16–F10 melanoma cells (5×10^5/mouse) were s.c. inoculated into C57BL/6 mice. Tim-3^+, PD-1^+, $CD44^{high}$, $CD103^+$, or $CXCR3^+$ $CD8^+$ T-cell subsets were gated, and the frequency of $CD147^+$ cells within each subset was analyzed with flow cytometry on day 15 after inoculation and is summarized in the right panel (5–8 mice per group). Markers are displayed in order and color-coded according to the frequency of $CD147^+$ cells. **D** scRNA-seq analysis of the transcript levels of Bsg, Pdcd1, and Havcr2 in cluster CD8_B relative to those in CD8_G or those in subcluster CD8_1 relative to those in other subclusters.[35] Data are representative of two independent experiments and are presented as the mean ± STD. *$P < 0.05$

proportion of apoptotic cells in $Bsg^{\triangle T}$ mice compared to Bsg^{WT} mice (Fig. 3A). This result suggested that the cytotoxic function of $CD8^+$ T cells might be involved in tumor inhibition induced by CD147 deficiency. With an anti-mouse CD8 antibody, we depleted $CD8^+$ T cells from Bsg^{WT} and $Bsg^{\triangle T}$ mice (Supplementary Fig. S2) and challenged the mice with B16–F10 cells. $CD8^+$ T-cell depletion almost completely abrogated the enhanced tumor control established by CD147 deficiency (Fig. 3B), indicating that direct killing of tumor cells by $CD8^+$ T cells is responsible for the antitumor effect induced by CD147 deficiency.

To validate the effects of CD147 deficiency on the effector function of $CD8^+$ T cells, we examined the expression of cytotoxicity-associated molecules in primary $CD8^+$ T cells upon TCR stimulation. The results showed that the proportions of IFN-γ-, TNF-α-, perforin-, and granzyme B-producing $CD8^+$ T cells were higher in $Bsg^{\triangle T}$ $CD8^+$ T cells than in Bsg^{WT} $CD8^+$ T cells (Fig. 3C). As expected, $Bsg^{\triangle T}$ $CD8^+$ T cells exhibited stronger cytotoxicity at an effector/target (E/T) ratio of 10:1 upon TCR stimulation than did Bsg^{WT} $CD8^+$ T cells in an ex vivo cytotoxicity analysis (Fig. 3D). These results suggest that CD147 deficiency

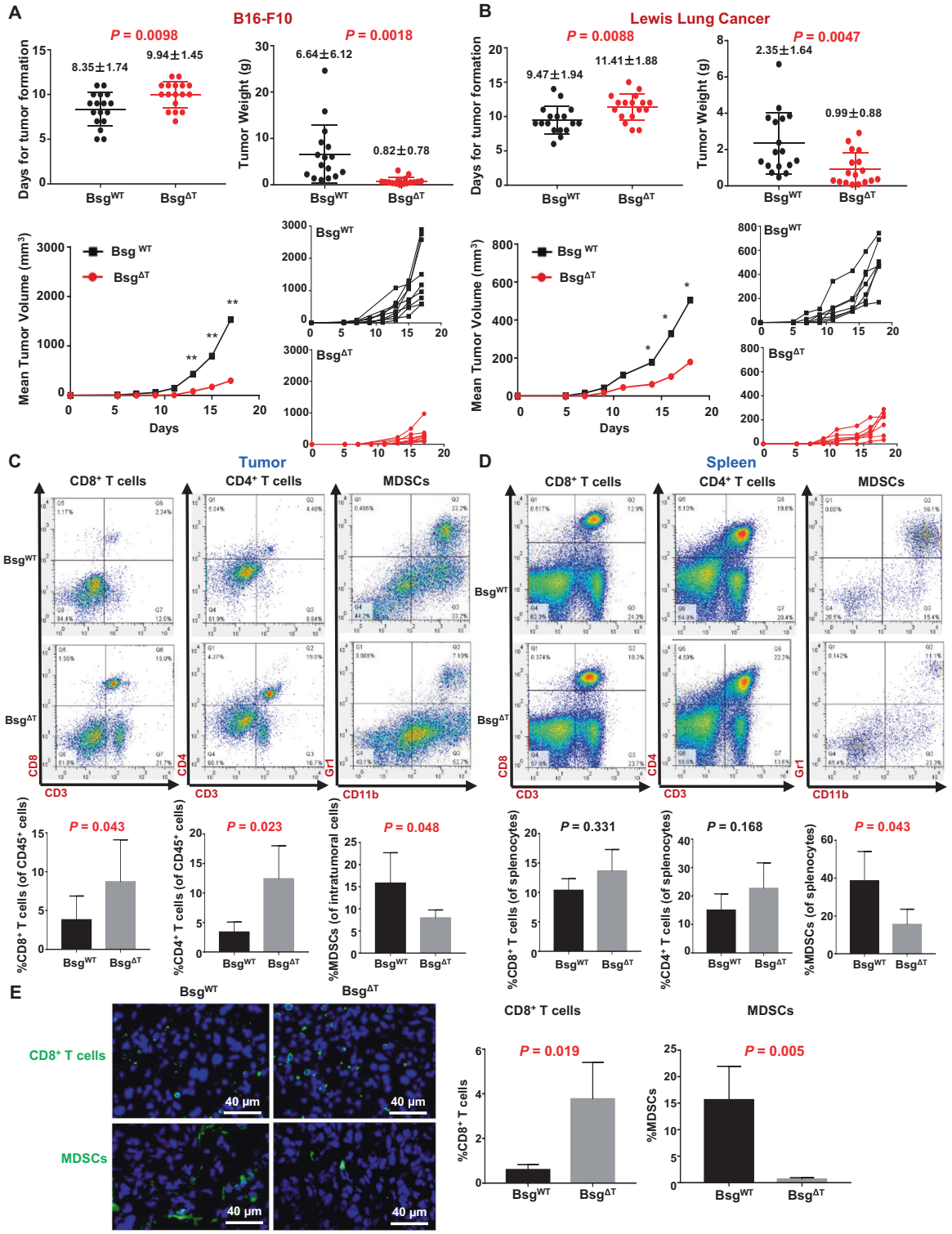

Fig. 2 CD147 deficiency in T cells inhibits tumor growth and enhances antitumor immunity. **A**, **B** Bsg^{WT} and Bsg$^{\Delta T}$ mice were s.c. inoculated with B16–F10 melanoma cells (5×10^5/mouse) (**A**) or LLC cells (1×10^6/mouse) (**B**). The days required for the formation of palpable tumor masses were recorded and are summarized on the left in the upper panel (16–17 pairs of mice). Tumor size was measured every other day starting on day 5, and tumors were weighed on day 17 (**A**) or day 18 (**B**) (17 pairs of mice). Individual tumor-growth curves are also shown on the right in the lower panel (7–9 pairs of mice). $^{**}P < 0.01$, $^{*}P < 0.05$. **C** The frequencies of CD8$^+$ T cells and CD4$^+$ T cells in the total tumor-infiltrating CD45$^+$ cell population and the MDSC frequency within LLC tumors from Bsg^{WT} or Bsg$^{\Delta T}$ mice analyzed by flow cytometry (six pairs of mice). **D** The frequencies of CD8$^+$ T cells, CD4$^+$ T cells, and MDSCs in spleens from LLC tumor-bearing Bsg^{WT} or Bsg$^{\Delta T}$ mice analyzed by flow cytometry (six pairs of mice). **E** Immunofluorescence staining of CD8$^+$ T cells or MDSCs within formalin-fixed paraffin-embedded tumor tissue samples from B16–F10 tumor-bearing Bsg^{WT} and Bsg$^{\Delta T}$ mice (three pairs of mice) with an anti-CD8a (green) or anti-Gr1 (green) antibody (RB6-8C5, reacting with a common epitope in Ly-6G and Ly-6C). The nuclei were stained with DAPI (blue). Data are representative of two independent experiments and are presented as the mean ± STD

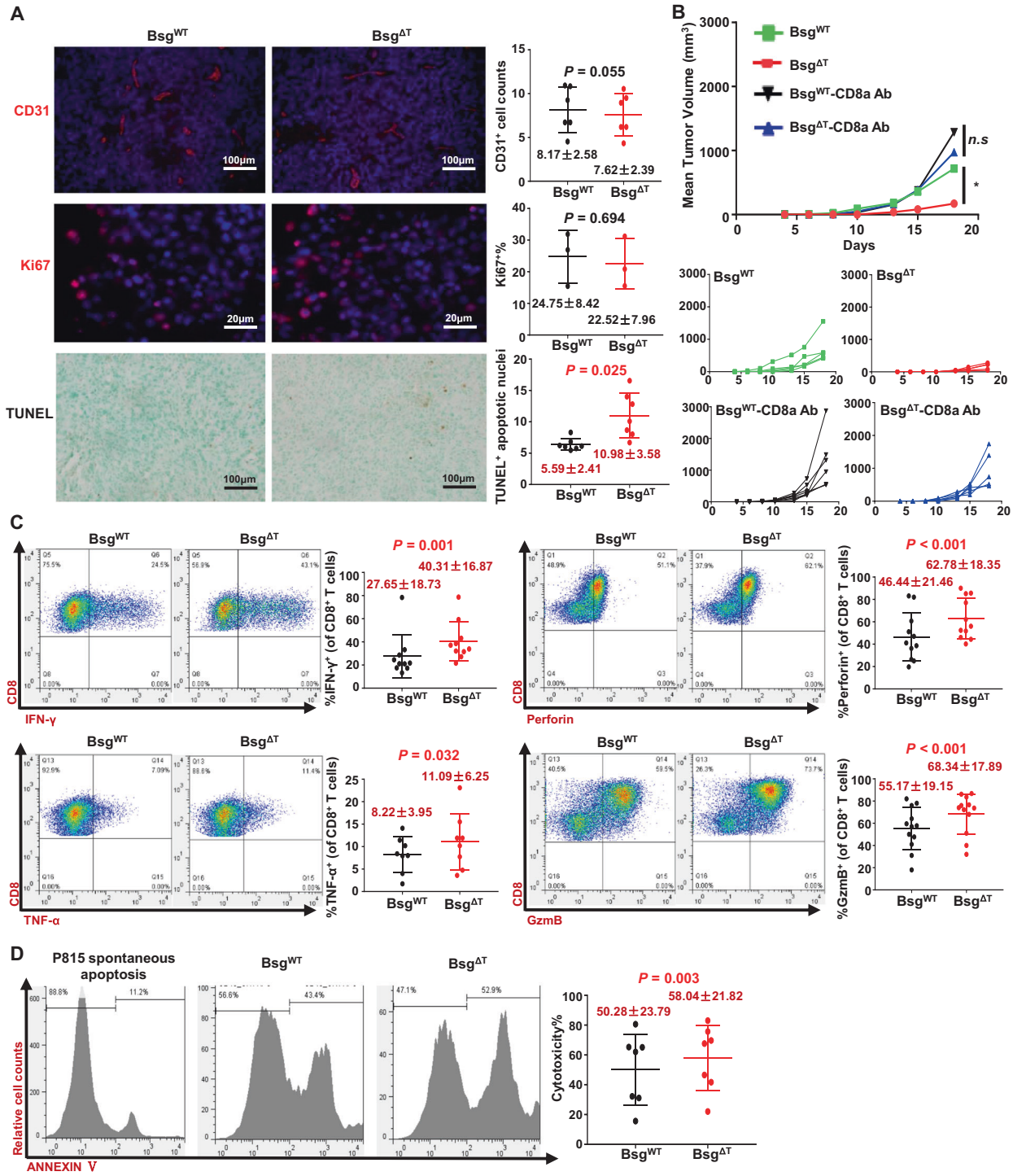

Fig. 3 CD147 deficiency augments the effector function of CD8$^+$ T cells. **A** Angiogenesis, proliferation, and apoptosis were analyzed in formalin-fixed paraffin-embedded tumor tissue samples from B16–F10 tumor-bearing Bsg^{WT} and Bsg$^{\Delta T}$ mice (3–7 pairs of mice) with immunofluorescence staining or the TUNEL method. The microvascular density and proliferating cells were labeled with an anti-CD31 (red) or anti-Ki67 (red) antibody, respectively. The nuclei were stained with DAPI (blue). Apoptotic cells (brown) were detected with TUNEL analysis. **B** B16–F10 melanoma cells (5×10^5/mouse) were s.c. inoculated into Bsg^{WT} and Bsg$^{\Delta T}$ mice, and the mice in the indicated groups were depleted of CD8$^+$ T cells by i.p. injection of 100 μg of anti-CD8a antibody on days 0 and 1 and twice weekly thereafter. Tumor growth was monitored every other day starting on day 5. Individual tumor-growth curves are shown in the lower panel (5–7 mice per group). Data are representative of two independent experiments. *$P < 0.05$. **C**, **D** Purified naive CD8$^+$ T cells isolated from the spleen of Bsg^{WT} and Bsg$^{\Delta T}$ mice were activated with anti-CD3/anti-CD28 antibodies for 40 h. **C** The frequencies of IFN-γ$^+$, TNF-α$^+$, perforin$^+$, and granzyme B$^+$ cells in the total CD8$^+$ T-cell population were analyzed with flow cytometry (8–12 pairs of mice). **D** For ex vivo cytotoxicity analysis, P815 cells were labeled with CFSE. Activated Bsg^{WT} or Bsg$^{\Delta T}$ CD8$^+$ T cells were incubated with an anti-CD3e antibody for 30 min, mixed with P815 cells at a 10:1 ratio, and incubated for 2 h. The cells were stained with ANNEXIN V-APC, and the frequency of ANNEXIN V$^+$ cells in the P815 cell population was analyzed with flow cytometry (seven pairs of mice, paired *t* test). Data are presented as the mean ± STD

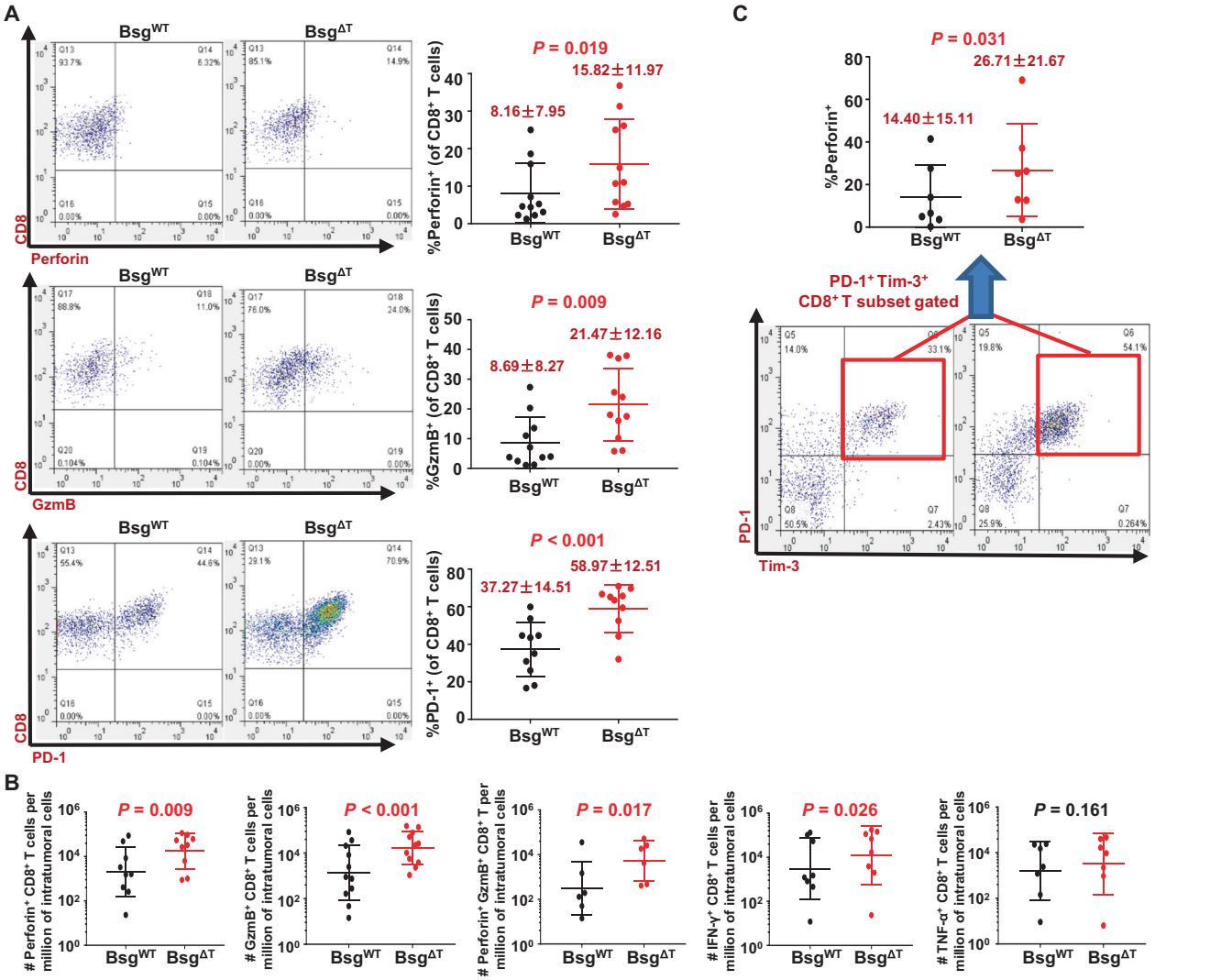

Fig. 4 CD147 deficiency increases the abundance of effector CD8$^+$ TILs within tumor tissues. **A** The frequencies of perforin$^+$, granzyme B$^+$, and PD-1$^+$ cells in the total tumor-infiltrating CD8$^+$ T-cell population in B16–F10 tumor-bearing Bsg^{WT} and Bsg$^{\Delta T}$ mice were analyzed with flow cytometry on day 15 after inoculation (10–11 pairs of mice). **B** The counts of perforin$^+$, granzyme B$^+$, IFN-γ$^+$, TNF-α$^+$, and perforin$^+$ granzyme B$^+$ tumor-infiltrating CD8$^+$ T cells per million total intratumoral cells in B16–F10 tumor-bearing Bsg^{WT} and Bsg$^{\Delta T}$ mice were calculated with flow cytometry on day 15 after inoculation (6–11 pairs of mice). **C** The frequency of perforin$^+$ cells in the PD-1$^+$ Tim-3$^+$ CD8$^+$ TIL population in B16–F10 tumor-bearing Bsg^{WT} and Bsg$^{\Delta T}$ mice was analyzed with flow cytometry on day 15 after inoculation (seven pairs of mice). Data are representative of two independent experiments and presented as the mean ± STD

enhances the effector function of CD8$^+$ T cells by upregulating cytotoxic molecule levels.

Similarly, in B16–F10 tumor-bearing Bsg$^{\Delta T}$ mice, the frequency of perforin-producing CD8$^+$ TILs was almost two times higher than that in Bsg^{WT} mice (Fig. 4A), and that of granzyme B-producing CD8$^+$ TILs was ~2.5 times higher than that in Bsg^{WT} mice (Fig. 4A). When normalized by using the total amounts of intratumoral cells as the denominator to eliminate the potential variable introduced by differences in tumor size at the time of collection, the counts of perforin-, granzyme B-, and IFN-γ-producing CD8$^+$ TILs and perforin$^+$ granzyme B$^+$ CD8$^+$ TILs were all significantly increased in Bsg$^{\Delta T}$ mice compared to Bsg^{WT} mice, with at least a tenfold increase observed for each subset (Fig. 4B). These results suggest that CD147 deficiency augments the effector function of CD8$^+$ TILs and the abundance of functional CD8$^+$ TILs.

Interestingly, the frequency of PD-1$^+$ CD8$^+$ TILs was also increased in Bsg$^{\Delta T}$ mice compared to Bsg^{WT} mice (Fig. 4A). As PD-1 is an identified marker for the repertoire of clonally expanded tumor-reactive or mutation-specific CD8$^+$ TILs,[36] this result indicates that CD147 deficiency may increase the tumor-reactive CD8$^+$ TIL population in the TME. It is known that coexpression of PD-1 and Tim-3 identifies exhausted T cells.[37] Here, we compared the functional status of PD-1$^+$ Tim-3$^+$ CD8$^+$ TIL subsets between B16–F10 tumor-bearing Bsg$^{\Delta T}$ and Bsg^{WT} mice. As determined by flow cytometry, we observed a significantly increased percentage of perforin-producing PD-1$^+$ Tim-3$^+$ CD8$^+$ TILs in the Bsg$^{\Delta T}$ mice (Fig. 4C), indicating that CD147 deficiency might partly reverse the dysfunctional status of PD-1$^+$Tim-3$^+$CD8$^+$ TILs.

To avoid environmental factors, such as the tumor burden, and other CD147-deficient T-cell subsets affecting CD8$^+$ T-cell differentiation and function in the conditional-knockout mouse model, we isolated CD147$^{+/+}$ CD8$^+$ T cells from wild-type CD45.1$^+$ mice and CD147$^{-/-}$ CD8$^+$ T cells from CD45.2$^+$ Bsg$^{\Delta T}$ mice and mixed them at a ratio of 1:1. The mixed cells were adoptively transferred into B16 melanoma-bearing RAG mice. Flow-cytometry analysis showed a significantly higher intratumoral abundance of

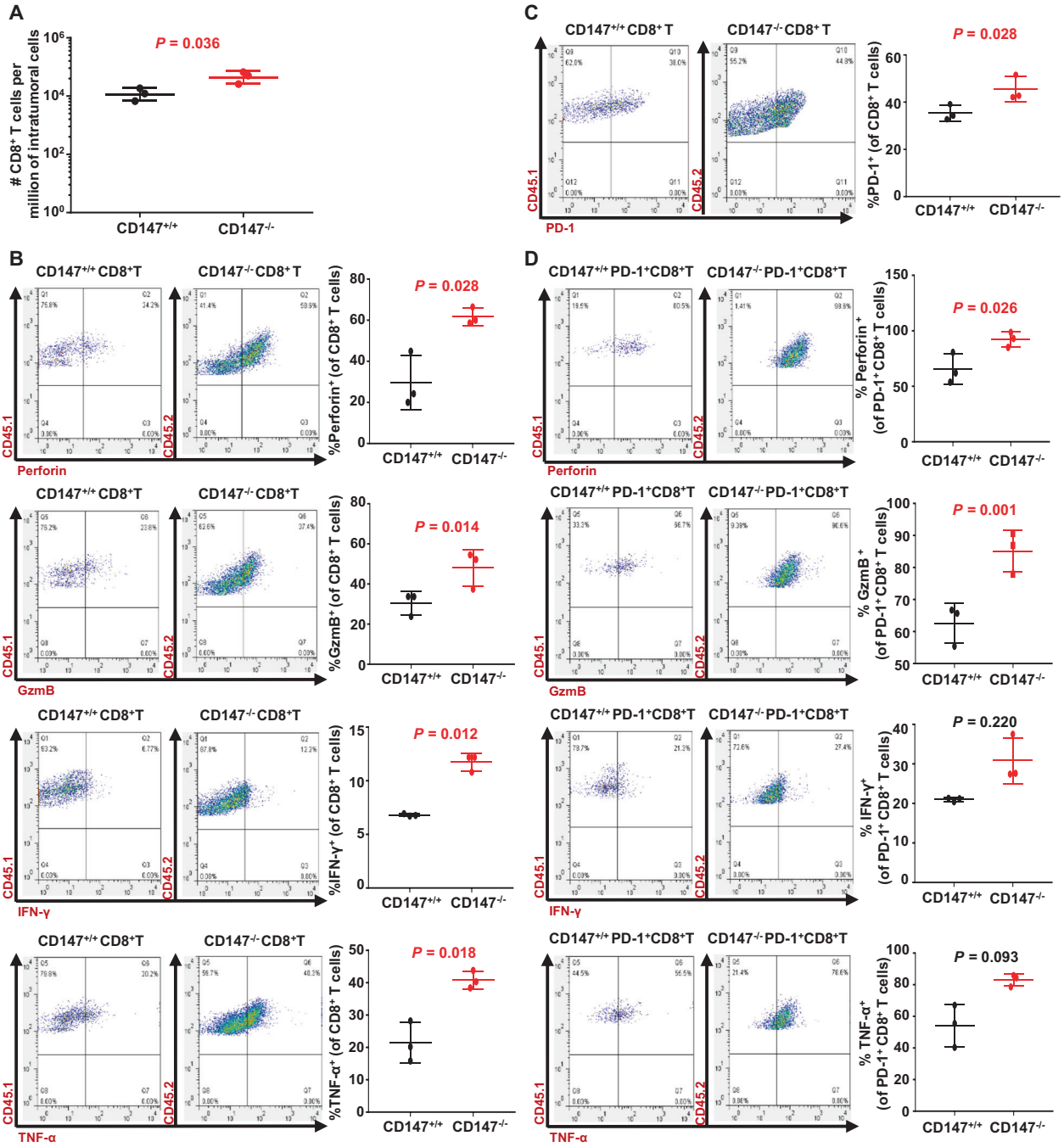

Fig. 5 CD147 deficiency increases the intratumoral abundance and effector function of CD8$^+$ TILs after adoptive transfer. **A** The counts of CD45.1$^+$ CD147$^{+/+}$ CD8$^+$ or CD45.2$^+$ CD147$^{-/-}$ CD8$^+$ T cells per million total intratumoral cells in recipient RAG mice were calculated with flow cytometry ($n = 3$). **B**, **C** The frequencies of perforin$^+$, granzyme B$^+$, IFN-γ$^+$, TNF-α$^+$, and PD-1$^+$ cells in the total CD45.1$^+$CD147$^{+/+}$ CD8$^+$ or CD45.2$^+$ CD147$^{-/-}$ CD8$^+$ TIL population were analyzed with flow cytometry ($n = 3$). **D** The frequencies of perforin$^+$, granzyme B$^+$, IFN-γ$^+$, and TNF-α$^+$ cells in the PD-1$^+$ CD45.1$^+$CD147$^{+/+}$ CD8$^+$ or PD-1$^+$ CD45.2$^+$ CD147$^{-/-}$ CD8$^+$ TIL population were analyzed with flow cytometry ($n = 3$)

CD45.2$^+$ CD147$^{-/-}$ CD8$^+$ TILs than that of CD45.1$^+$ CD147$^{+/+}$ CD8$^+$ TILs (Fig. 5A). The frequencies of perforin-, granzyme B-, IFN-γ-, and TNF-α-producing CD45.2$^+$ CD147$^{-/-}$ CD8$^+$ TILs were higher than those of the corresponding CD45.1$^+$ CD147$^{+/+}$ CD8$^+$ TILs, with approximately twofold increases (Fig. 5B). Similarly, the frequency of the PD-1$^+$ subset was also increased in CD45.2$^+$ CD147$^{-/-}$ CD8$^+$ TILs compared to CD45.1$^+$ CD147$^{+/+}$ CD8$^+$ TILs (Fig. 5C), and the CD45.2$^+$ population exhibited superior effector function (Fig. 5D).

Runx3 and T-bet mediate CD147 deficiency-induced antitumor CD8$^+$ T-cell responses

To investigate the molecular mechanism underlying the enhanced effector function of CD8$^+$ T cells induced by CD147 deficiency, we analyzed the expression of three known cytotoxic transcription factors, Runx3, T-bet, and Eomes, in CD8$^+$ T cells. Upon TCR stimulation, a higher proportion of intranuclear Runx3- or T-bet-expressing CD8$^+$ T cells was found in Bsg$^{\triangle T}$ CD8$^+$ T cells than in Bsg^{WT} CD8$^+$ T cells (Fig. 6A), while the proportion of

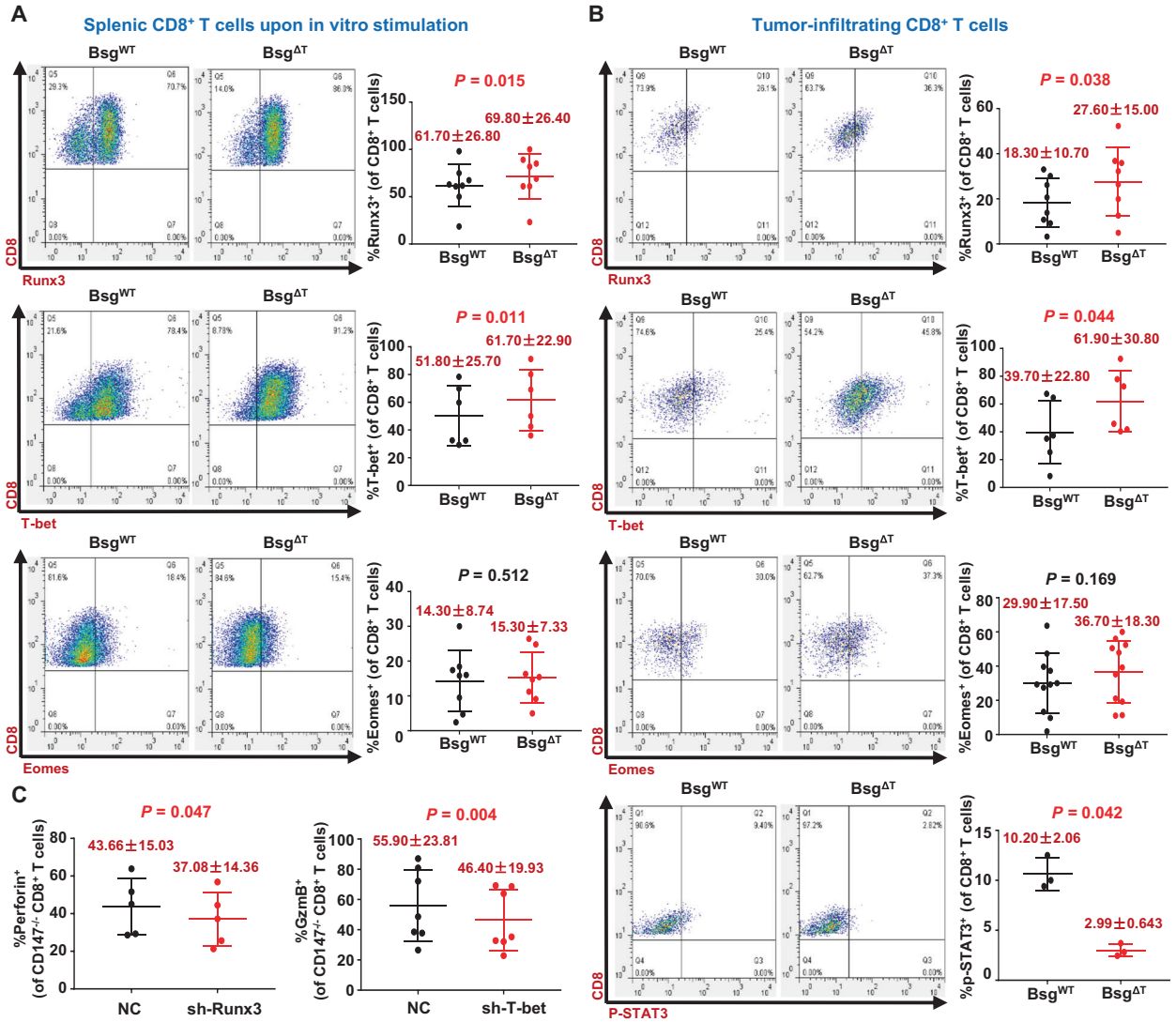

Fig. 6 Runx3 and T-bet mediate CD147 deficiency-induced antitumor CD8$^+$ T-cell responses. **A** Purified CD8$^+$ T cells isolated from the spleen of Bsg^{WT} and Bsg$^{\Delta T}$ mice were activated with anti-CD3/anti-CD28 antibodies for 40 h. The frequencies of Runx3$^+$, T-bet$^+$, and Eomes$^+$ cells in the total CD8$^+$ T-cell population were analyzed with flow cytometry (6–8 pairs of mice). **B** B16–F10 melanoma cells (5×10^5/mouse) were s.c. inoculated into Bsg^{WT} and Bsg$^{\Delta T}$ mice. The frequencies of Runx3$^+$, T-bet$^+$, Eomes$^+$, and p-STAT3$^+$ cells in the total tumor-infiltrating CD8$^+$ T-cell population of the Bsg^{WT} and Bsg$^{\Delta T}$ mice were analyzed with flow cytometry on day 15 after inoculation (6–11 pairs of mice). Data are representative of two independent experiments. **C** CD8$^+$ T cells purified from the spleen of Bsg$^{\Delta T}$ mice (5–7 mice) were activated with anti-CD3/anti-CD28 antibodies for 24 h and then transduced with retroviruses encoding Runx3-specific shRNA, T-bet-specific shRNA, or negative control shRNA (NC). Left, the proportion of perforin$^+$ cells in the CD8$^+$ T cells transduced with NC or Runx3-specific shRNA. Right, the proportion of granzyme B$^+$ cells in the CD8$^+$ T cells transduced with NC or T-bet-specific shRNA. Data are represented as the mean ± STD

Eomes-expressing CD8$^+$ T cells was nearly unaffected by CD147 deficiency in CD8$^+$ T cells (Fig. 6A). Similarly, in B16–F10 tumor-bearing Bsg$^{\triangle T}$ mice, the frequencies of intranuclear Runx3-expressing CD8$^+$ TILs and T-bet-expressing CD8$^+$ TILs were approximately 1.5 times higher than those in Bsg^{WT} mice (Fig. 6B), whereas no difference in the frequency of Eomes-expressing CD8$^+$ TILs was found between Bsg$^{\triangle T}$ and Bsg^{WT} mice (Fig. 6B), suggesting that Runx3 and T-bet but not Eomes may be involved in the enhanced cytotoxic function of CD8$^+$ TILs induced by CD147 deficiency. In addition, CD147 deficiency in CD8$^+$ TILs led to a reduction in the p-STAT3 level (Fig. 6B), which might potentially repress cytotoxic genes by interfering with the functions of T-bet and Runx3.

To further study the effects of the transcription factors Runx3 and T-bet on the effector function of CD147$^{-/-}$ CD8$^+$ T cells, we knocked down Runx3 or T-bet expression in activated primary CD147$^{-/-}$ CD8$^+$ T cells with retroviruses encoding Runx3- or T-bet-specific shRNA, respectively, and analyzed the knockdown efficiency with RT-PCR (Supplementary Fig. S3a). Compared with CD147$^{-/-}$ CD8$^+$ T cells transduced with control retroviruses, cells with Runx3 knockdown showed a reduced frequency of perforin$^+$ CD8$^+$ T cells, while cells with T-bet knockdown had a reduced frequency of granzyme B$^+$ CD8$^+$ T cells (Fig. 6C). Although a previous study showed reduced expression of granzyme B upon Runx3 deficiency in a mouse model of acute infection,[38] knockdown of Runx3 expression in CD147$^{-/-}$ CD8$^+$ T cells did not influence the expression of granzyme B nor did knockdown of T-bet impact perforin expression (Supplementary Fig. S3b). These results suggest that Runx3 and T-bet mediate the enhanced effector function of CD8$^+$ T cells induced by CD147 deficiency, but may depend on different regulatory mechanisms.

As Runx3 has been recently identified as a central regulator of tissue-resident memory CD8$^+$ T (T_{RM}) cell differentiation in CD8$^+$ TILs,[39] and our findings showed that CD147 deficiency led to an

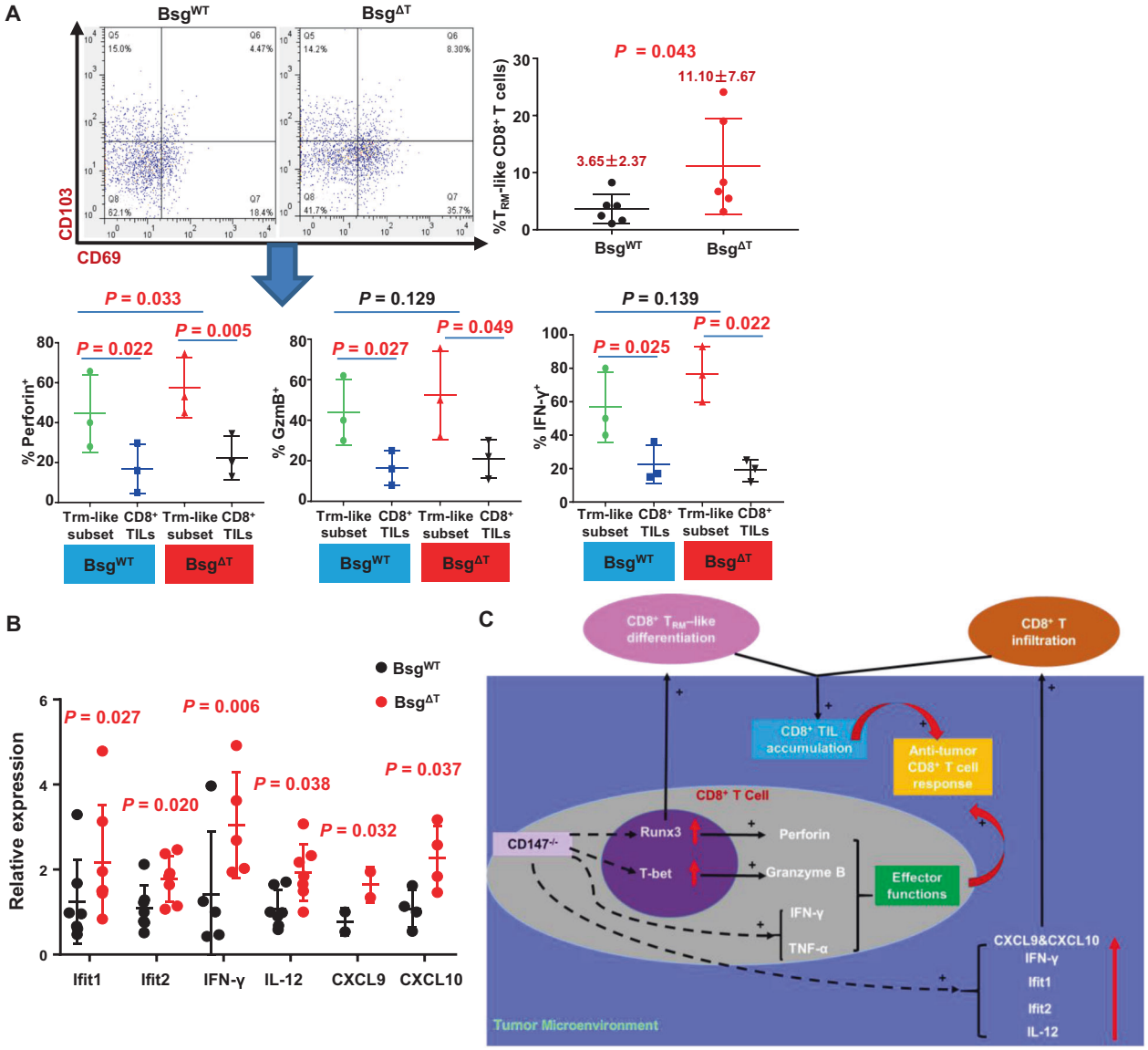

Fig. 7 CD147 deficiency shifts the T_{RM} program and tumor-immune phenotype. **A**, **B** B16–F10 melanoma cells (5×10^5/mouse) were s.c. inoculated into Bsg^{WT} and Bsg$^{\Delta T}$ mice. **A** The frequency of T_{RM}-like cells in the total tumor-infiltrating CD8$^+$ T-cell population of Bsg^{WT} and Bsg$^{\Delta T}$ mice was analyzed with flow cytometry on day 15 after inoculation (six pairs of mice). The frequencies of perforin$^+$, granzyme B$^+$, and IFN-γ$^+$ cells in the T_{RM}-like cell or CD8$^+$ TIL population were analyzed with flow cytometry (three pairs of mice). **B** The levels of mRNA transcripts encoding known antitumor-immune mediators in tumors from Bsg^{WT} and Bsg$^{\Delta T}$ mice were assessed by quantitative RT-PCR (3–6 pairs of mice). The relative expression of each gene is shown normalized to the expression of β-actin. **C** Model of CD8$^+$ T-cell-immune modulation by CD147 deficiency. Data are representative of two independent experiments and presented as the mean ± STD

increase in CD8$^+$ TIL numbers (Figs. 2C and 5A), we speculated that the impact of CD147 on CD8$^+$ TIL accumulation may involve T_{RM}-like cell retention and differentiation driven by Runx3. We examined the key tissue-retention molecules CD103 and CD69 (markers of T_{RM} cells) with flow cytometry. The results showed that in accordance with the increased percentage of CD8$^+$ TILs, CD147 deficiency resulted in an increased abundance of CD69$^+$ CD103$^+$ T_{RM}-like cells (Fig. 7A). When comparing the expression of effector-function molecules (perforin, granzyme B, and IFN-γ) between the CD69$^+$CD103$^+$ CD8$^+$ T_{RM}-like subset and CD8$^+$ TILs, we found that the T_{RM}-like cells were significantly functionally superior to CD8$^+$ TILs, as shown in Fig. 7A.

The chemotaxis system is another factor influencing the abundance of CD8$^+$ TILs within tumors. Here, we found that the mRNA levels of the interferon-inducible chemokines CXCL9 and CXCL10 were increased in fresh tumor tissue samples isolated from Bsg$^{\triangle T}$ mice (Fig. 7B), suggesting that the chemotaxis environment in the TME of Bsg$^{\triangle T}$ mice may be stronger than that in Bsg^{WT} mice, which may partly contribute to the increased abundance of CD8$^+$ TILs in Bsg$^{\triangle T}$ mice. Accordingly, CD147 deficiency markedly increased the levels of mRNAs encoding IFN-γ, an inducer of CXCL9 and CXCL10; IFN-γ induced IL-12, and Ifit1 and Ifit2, two type I IFN-stimulated genes (ISGs) (Fig. 7B); these results reflected enhanced type I interferon signaling-mediated chemotaxis and antitumor immunity in Bsg$^{\triangle T}$ tumors, which are known to be central to immune-mediated tumor control.

CD147 expression on CD8$^+$ TILs is correlated with the clinicopathological characteristics of NSCLC patients

To examine whether CD147 could be a potential target for cancer immunotherapy, we assessed the expression of CD147 on CD8$^+$ TILs in tumor tissue samples from patients with NSCLC. As CD147 is

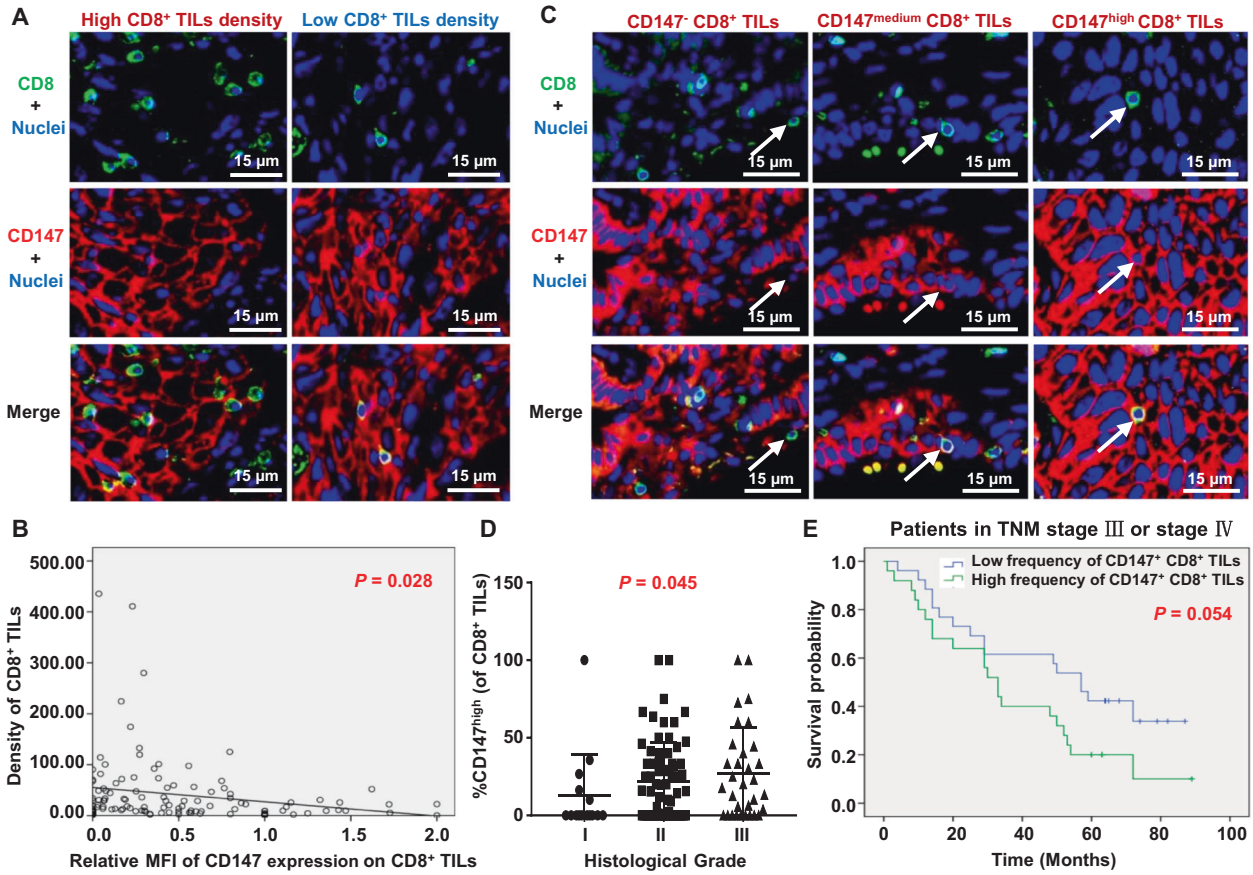

Fig. 8 Correlations between the CD147 expression on $CD8^+$ TILs and clinicopathological characteristics of non-small-cell lung cancer (NSCLC) patients. **A** Representative figures of double-immunofluorescence staining for $CD147^+$ $CD8^+$ TILs in NSCLC tumor tissue samples with a high or low $CD8^+$ TIL density using anti-CD8a (green) and anti-CD147 (red) antibodies. The nuclei were stained with DAPI (blue). **B** The correlation between the MFI of CD147 staining on $CD8^+$ TILs and the $CD8^+$ TIL density was determined with linear- regression analysis ($n = 117$). **C** Representative images of $CD147^-$ $CD8^+$, $CD147^{medium}$ $CD8^+$, and $CD147^{high}$ $CD8^+$ TILs. Arrow, a representative $CD8^+$ TIL. **D** The correlation between the frequency of intratumoral $CD147^{high}$ $CD8^+$ TILs and histological grade was determined with Spearman correlation analysis ($n = 117$). **E** The overall survival of NSCLC patients with TNM-stage III or IV disease was compared between the group with a high frequency of $CD147^+$ $CD8^+$ TILs (>24.64%) and the group with a low frequency (≤24.64%) with the Kaplan–Meier method and log-rank test ($n = 51$)

well known to be highly expressed on cancer cells, we employed the immunofluorescence double-staining method with an anti-CD8a antibody and an anti-CD147 antibody, and quantified the expression of CD147 on $CD8^+$ cells in tissue microarrays containing tumor samples from 117 NSCLC patients (Fig. 8A).

$CD8^+$ TILs could be detected in all 117 NSCLC tumor samples, and 85.47% of the samples contained $CD147^+CD8^+$ TILs with a median $CD147^+CD8^+$ TIL frequency of 24.63% (ranging from 0 to 100%). In further analysis, the frequency of $CD147^+CD8^+$ TILs was treated as a continuous variable and compared between different subgroups of major clinicopathological variables, as shown in Table 1. Overall, no associations between the frequency of $CD147^+CD8^+$ TILs and major clinicopathological variables (age, histological subtype, TNM stage, and tumor diameter) were found (Table 1).

As CD147 gene deletion increased the abundance of TILs in our murine models, we explored whether the expression of CD147 influences the abundance of $CD8^+$ TILs in NSCLC patients. With correlation analysis, a negative correlation was found between the density of $CD8^+$ TILs and the mean fluorescence intensity (MFI) of CD147 staining on $CD8^+$ TILs. The higher the MFI of CD147 expression on $CD8^+$ TILs was, the lower the abundance of $CD8^+$ TILs (Fig. 8B).

To further elucidate the effects of CD147 expression on $CD8^+$ TILs, we divided $CD147^+CD8^+$ TILs into two subgroups, $CD147^{high}$ and $CD147^{medium}$ $CD8^+$ TILs, according to the fluorescence intensity of CD147 expression (Fig. 8C). Considering that the functional status of $CD8^+$ TILs in tumor islets may be different from that of $CD8^+$ TILs in stromal regions, we calculated the density and CD147 expression of intratumoral and stromal $CD8^+$ TILs separately (Supplementary Fig. S4a) and compared them between different subgroups of major clinicopathological variables and histological tumor grades. Only the frequency of intratumoral $CD147^{high}$ $CD8^+$ TILs was found to be associated with histological grade among all the variables (Fig. 8D and Table 1). The higher the degree of malignancy was, the higher the frequency of intratumoral $CD147^{high}$ $CD8^+$ TILs, indicating that CD147 may be involved in crosstalk between $CD8^+$ TILs and cancer cells, contributing to the immunoediting mediated by $CD8^+$ TILs in tumor islets.

With the Kaplan–Meier method and log-rank test, we analyzed the effects of $CD147^+CD8^+$ TILs and $CD8^+$ TILs on the overall survival (OS) of these patients. The frequency of $CD147^+CD8^+$ TILs was stratified as "high" (>24.64% of $CD8^+$ TILs) or "low" (≤24.64% of $CD8^+$ TILs). The density of $CD8^+$ TILs was stratified as "high" (>22.60, the median density) or "low" (≤22.60). The results showed that for the patients with TNM-stage III or IV disease, a high frequency of $CD147^+CD8^+$ TILs was marginally associated with poor survival ($P = 0.054$, Fig. 8E); in contrast, no association was found between the density of $CD8^+$ TILs and OS ($P = 0.246$, Supplementary Fig. S4b), although a tendency toward better survival with a high $CD8^+$ TIL density seemed to exist.

Table 1. Correlations between the CD147 expression on CD8$^+$ TILs and clinicopathological characteristics of NSCLC patients

	Number	CD147$^+$CD8$^+$ % (median)	*P* value	Intratumoral CD147^{high}CD8$^+$% (median)	*P* value
Sex					
Male	87	27.94	0.020	16.00	0.227
Female	30	9.903		0.588	
Age (years)					
<65	60	24.82	0.647	18.70	0.250
≥65	57	22.22		9.091	
Histology					
ADC	52	29.11	0.413	14.36	0.946
SCC	65	20.46		14.29	
TNM stage					
I+II	66	23.61	0.802	9.545	0.151
III+IV	51	24.64		17.65	
Tumor diameter					
<4 cm	48	26.09	0.727	7.323	0.230
≥4 cm	69	22.22		17.65	

ADC adenocarcinoma, *SCC* squamous cell carcinoma
P values were determined using the Wilcoxon rank test or Kruskal–Wallis H test

Overall, these results indicated that expression of CD147 on CD8$^+$ TILs might decrease the abundance of CD8$^+$ TILs, correlate with low-differentiation tumors, and lead to a poor clinical outcome in advanced NSCLC patients.

DISCUSSION

In this study, we reported that CD147 expression was significantly upregulated on CD8$^+$ TILs, and that CD147 was coexpressed with PD-1 and Tim-3 in the TME and contributed to impaired antitumor-immune responses mediated by CD8$^+$ TILs by inhibiting the accumulation and effector function of CD8$^+$ TILs partly through regulation of the cytotoxic transcription factors Runx3 and T-bet (Fig. 7C). T-cell CD147 deficiency was sufficient to limit tumor growth in a CD8$^+$ T-cell-dependent manner and could partly reverse the dysfunctional status of PD-1$^+$Tim-3$^+$CD8$^+$ TILs. As the importance of CD147 to CD8$^+$ T cells and antitumor immunity remains unknown, these results are the first to identify CD147 as a negative regulator of the effector function of CD8$^+$ TILs and a potential candidate target for cancer immunotherapy.

CD147 expression has been reported to be upregulated on activated lymphocytes upon in vitro stimulation or under inflammatory conditions,[40,41] but the function of CD147 on T cells remains controversial. Although some in vitro studies describe CD147 as a negative regulator of CD4$^+$ T cells,[32,33] other reports have concluded that antibody-induced inhibitory effects on T cells occur via blockade of CD147,[24] and that CD147 silencing could reduce the expression of CD25 and CD69 on memory CD4$^+$ T cells.[42] In this study, we found that the tumor burden could upregulate CD147 expression on splenic T cells, while in the TME, only the expression of CD147 on CD8$^+$ TILs was further increased, and CD147 was coexpressed with the inhibitory receptors PD-1 and Tim-3. Conditional deletion of *Bsg* in Lck-cre-expressing T cells was found to influence early thymocyte development[33,43] and age-related thymic involution,[44] but had little impact on the numbers and activation state of peripheral T cells[33] in mature mice (8–12-week-old) in our previous studies, which was in accordance with our findings shown in Fig. 2D and Supplementary Fig. S1a (with 8–10-week-old mice). Furthermore, to avoid the possible influence of lck-driven Cre expression on peripheral T-cell states,[45] we compared the tumor control efficiency and effector function of CD8$^+$ TILs among littermates with the genotypes Bsg$^{\Delta T}$, Bsg^{WT}, and Lck-cre;Bsg$^{WT/WT}$ and found no significant differences in the tumor control or effector function of CD8$^+$ TILs between the Bsg^{WT} and Lck-cre; Bsg$^{WT/WT}$ mice (Supplementary Fig. S5), suggesting that lck-driven Cre expression would not interfere with the effects of CD147 deletion. With this conditional-knockout mouse model, we found that genetic deletion of CD147 in T cells profoundly controlled tumor growth and enhanced antitumor immunity. Although the effects of CD147 deficiency on CD4$^+$ T cells and innate NK-like lineages[43] also possibly impact the TME and antitumor immunity, our results showing that adoptive transfer of isolated Bsg$^{\triangle T}$ CD8$^+$ T cells exhibited enhanced effector function, and that depletion of CD8$^+$ T cells nearly abrogated the enhancement in antitumor immunity induced by CD147 deficiency in Bsg$^{\triangle T}$ mice, indicated that CD147 expression on the CD8$^+$ lineage has an indispensable impact on the negative regulation of antitumor immunity.

The transcription factor Runx3 has been identified as a key module in the transcriptional network that allows activated CD8$^+$ T cells to fully acquire cytotoxic functions,[46] and T-bet has been identified as the "master regulator" of cytotoxic transcriptional factors, cooperating with Runx3 to orchestrate effector CD8$^+$ T-cell differentiation.[38] Our results suggest that CD147 may be an upstream regulator of Runx3 and T-bet that influences the effector function of CD8$^+$ T cells. CD147 deficiency increased the levels of Runx3 and T-bet in vitro and in vivo, and enhanced the expression of the cytotoxic effector molecules perforin and granzyme B, but had no impact on Eomes. Gene knockdown of Runx3 or T-bet partly abrogated the enhanced expression of perforin or granzyme B in CD8$^+$ T cells induced by CD147 deficiency. CD147 has been recognized as a cell-surface signal transduction molecule. For example, CD147 can activate the signaling molecule STAT3, which has been reported to repress the expression of cytotoxic genes, including those encoding granzyme B, IFN-γ, and T-bet,[47] indicating that STAT3 may mediate the effects of CD147 on T-bet or cytotoxic molecules. In the present study, CD147 deficiency significantly decreased the level of p-STAT3 in CD8$^+$ TILs (Fig. 6B), supporting the conclusion that CD147 may inhibit T-bet by activating STAT3 in CD8$^+$ TILs. The detailed mechanisms underlying how CD147 regulates STAT3, Runx3, and T-bet merit further study.

In addition to the effects on cytotoxic function, our results from a murine tumor model and patient tumor samples suggested that CD147 may play a role in the accumulation of CD8$^+$ TILs. Runx3 has been recently identified as a central regulator of T_{RM} differentiation in multiple nonlymphoid sites, and is required for CD8$^+$ TIL accumulation in the TME.[39] CD147 deficiency increased the frequencies of Runx3$^+$ CD8$^+$ TILs and T_{RM}-like cells, which may be partly responsible for the enhanced TIL accumulation. Moreover, T_{RM}-like cells were found to be functionally superior to CD8$^+$ TILs (Fig. 7A). As manipulation of T_{RM} differentiation can not only foster the accumulation of TILs but also potentiate TIL cytotoxicity,[48] we infer that the signaling pathways underlying the cytotoxic effector program and T_{RM} program may be inseparably interconnected, with CD147 potentially serving as a signaling hub mediator. Additionally, the chemokines CXCL9 and CXCL10 can shift the tumor-immune phenotype into a "hot" (inflamed) profile by promoting effector T-cell trafficking into the TME and amplifying the immune response.[49] The increased levels of CXCL9 and CXCL10 observed upon CD147 deficiency might also contribute to the enhanced accumulation of TILs.

CD8$^+$ TILs represent preexisting antitumor-immune responses and are reported to correlate with the prognosis of cancer patients in some studies. Here, in advanced NSCLC patients (TNM-stage III or IV), the patients with a higher CD8$^+$ TIL density seemed to have

a better prognosis, but the improvement was not statistically significant. When considering the expression of CD147 on CD8$^+$ TILs, a marginal association between a higher frequency of CD147$^+$ CD8$^+$ TILs and a worse prognosis was found, suggesting that CD147 may negatively regulate the function of CD8$^+$ TILs and facilitate the precise understanding of the clinical significance of CD8$^+$ TIL subsets. The association between CD147$^+$ CD8$^+$ TILs and prognosis warrants further study in a larger cohort of cancer patients.

In our syngeneic tumor models, ~40% of CD8$^+$ TILs were CD147 positive, while in NSCLC patient tumor tissue samples, 85.47% of the samples contained CD147$^+$CD8$^+$ TILs with a median frequency of 24.63%. Therefore, CD147 blockade may be a potential applicable strategy for cancer immunotherapy. Additionally, CD147 was coexpressed with PD-1 and Tim-3 on CD8$^+$ TILs. PD-1 inhibits T-cell functions via the immunoreceptor tyrosine-based switch motif (ITSM) in its cytoplasmic tail.[50] CD147, in contrast, has a short cytoplasmic domain without an ITSM motif. CD147 and PD-1 come from diverse structural families and have distinct signaling domains and patterns of downstream signaling. CD147 deficiency could increase the frequency of PD-1$^+$ CD8$^+$ TILs and rescue the functional status of PD-1$^+$ Tim-3$^+$ CD8$^+$ TILs. Thus, CD147 and PD-1 may exert inhibitory effects via nonredundant pathways and cooperatively promote T-cell dysfunction. In addition, conversion of a "cold" TME into a "hot" TME upon CD147 deficiency, as mentioned above, may help reshape the cancer-immune phenotype,[49] providing an opportunity to increase the therapeutic efficacy of immune-checkpoint blockade.[51] Whether dual blockade of PD-1 and CD147 on T cells could have additive effects to reinvigorate antitumor CD8$^+$ TILs warrants further study and is being studied in our lab.

In summary, our study revealed a novel role for CD147 as a negative regulator of the effector function and intratumoral abundance of CD8$^+$ TILs. Novel therapeutic strategies developed to interfere with the function of CD147 may hold new promise for improving the outcome of cancer immunotherapy.

MATERIALS AND METHODS

Mice and tumor cell lines

Eight- to ten-week-old mice were used for all experiments. C57BL/6 mice were purchased from the Laboratory Animal Center of Fourth Military Medical University. Bsg$^{\triangle T}$ (Ick-cre; Bsg$^{flox/flox}$) and Bsg^{WT} (Bsg$^{flox/flox}$) mice on the C57BL/6 background were generated previously in our laboratory, and only paired littermates from the same breeding colony were used for experiments. All mice were housed under specific pathogen-free conditions at the Laboratory Animal Center of Fourth Military Medical University. Animal studies were approved by the Laboratory Animal Ethics Committee of Fourth Military Medical University, and all experiments were performed in accordance with national ethical guidelines as defined by the relevant national animal welfare bodies.

The B16–F10 and Lewis lung cancer cell lines were obtained from the Institute of Cell Biology, Chinese Academy of Sciences (Shanghai, China), and maintained in Dulbecco's minimal essential medium containing 10% fetal bovine serum (FBS) in a humidified 37 °C incubator with 5% CO_2.

Syngeneic tumor models

Tumor cells were harvested by trypsinization, and cell viabilities greater than 95% were confirmed by trypan blue exclusion. A total of 5×10^5 B16–F10 or 1×10^6 Lewis lung cancer cells were s.c. inoculated into the left flank of mice in 100 μl of PBS. The tumor-formation time was recorded and defined as the time when tumor masses reached palpable growth with a diameter of ~5 mm. For CD8$^+$ T-cell depletion, mice were given 100 μg of anti-CD8a antibody (53-6.7, BioLegend, UK) by i.p. injection on days 0 and 1 and twice per week thereafter. Tumor growth was monitored every other day, and tumor volumes were calculated using the equation $V = 4\pi (L_1 \times L_2)/3$, where V = volume ($mm^3$), L_1 = longest radius (mm), and L_2 = shortest radius (mm). Mice were sacrificed at experimental end points, and spleens and tumors were excised. Tumors were photographed and weighed before the next step.

Preparation of cell suspensions and flow cytometry

Spleens harvested from mice were mechanically disrupted and further dissociated through a 70-μm nylon cell strainer (BD Falcon, USA). Then, the red blood cells were lysed with blood cell lysis buffer (0.14 M NH_4Cl in HEPES, pH 7.0). For analysis of TILs, tumors were cut into small pieces (<3 mm) and incubated in a dissociation solution (RPMI medium supplemented with collagenase type I (200 U/ml) and DNase I (100 μg/ml)) for 30 min at 37 °C. Tumor tissue was dispersed into a single-cell suspension, and TILs were enriched using Mouse CD45 Positive Isolation Microbeads (Miltenyi Biotec, Germany) when needed, according to the manufacturer's instructions.

For surface molecule staining, cells were incubated with the following fluorochrome-conjugated antibodies: anti-CD3e (145-2C11), anti-CD8a (53-6.7), anti-CD4 (RM4–5), anti-CD44 (IM7), anti-CD147 (RL73), anti-PD-1 (J43), anti-Tim-3 (5D12), anti-CD69 (H1.2F3), anti-CD103 (M290), anti-CXCR3 (CXCR3-173), anti-Gr1 (RB6-8C5), or anti-CD11b (M1/70) from BD Bioscience (San Diego, CA, USA), and anti-CD45.1 (A20), anti-CD45.2 (104) or anti-CD25 (PC61) from BioLegend (USA). For intracellular cytokine staining, CD8$^+$ T cells were stimulated ex vivo for 5 h with phorbol 12-myristate 13-acetate, ionomycin, and Brefeldin A (Cell Activation Cocktail, BD Bioscience, USA) and permeabilized with the Cytofix/Cytoperm Kit (BD Bioscience, USA), followed by incubation with the following antibodies: anti-IFN-γ (REA638) and anti-TNF-α (MP6-XT22) from Miltenyi Biotec (Germany) and anti-perforin (eBioO-MAK-D) and anti-granzyme B (NGZB) from eBioscience (San Diego, CA, USA). For the detection of transcription factors, surface-stained cells were fixed and permeabilized with the Transcription Factor Staining Buffer Set (eBioscience, USA). Then, the cells were stained with fluorochrome-conjugated antibodies against Runx3 (R3-5G4, BD, USA), T-bet (REA102, Miltenyi, Germany), or Eomes (REA116, Miltenyi, Germany). For the detection of p-STAT3, surface-stained cells were fixed with IC Fixation Buffer (eBioscience, USA), followed by permeabilization with prechilled methanol for at least 30 min at 4 °C. Then, the cells were stained with fluorochrome-conjugated antibodies against p-STAT3 (LUVNKLA, eBioscience, USA). At least 2 million events were collected during flow-cytometric analysis using a FACSCalibur flow cytometer (BD, USA) and analyzed using FlowJo software (Tree Star Inc.).

Immunofluorescence staining

Immunofluorescence staining was performed as described previously.[52] Briefly, slides were deparaffinized and subjected to antigen retrieval using sodium citrate buffer (pH = 6.0) with boiling for 20 min in a pressure cooker. After incubation with a blocking solution containing 5.0% bovine serum albumin in a 0.3% Tween solution for 30 min, the murine tumor tissue slides were incubated with a rat anti-CD8a (1:100, clone 53-6.7, BD Bioscience, USA), rat anti-Ly-6G/Ly-6C (1:200, clone RB6-8C5, Thermo Fisher Scientific, USA), rabbit anti-CD31 (1:200, polyclonal, Abcam, USA), or mouse anti-ki67 antibody (1:200, clone SP6, Abcam, USA), while the tissue microarrays were incubated with mouse anti-CD8a (1:200, clone C8/144B, Abcam, USA) and rabbit anti-CD147 (1:200, polyclonal, Abcam, USA) antibodies overnight at 4 °C. After three washes with PBS, the slides were incubated with a donkey anti-rat Alexa Fluor 488-conjugated (1:200), goat anti-rabbit Alexa Fluor 594-conjugated (1:400), donkey anti-mouse Alexa Fluor 594-conjugated (1:400), or goat anti-mouse Alexa Fluor 488-conjugated (1:200) antibody from Thermo Fisher Scientific (USA) for 2 h at room temperature (RT). Nuclei were stained with

4′,6-diamidino-2-phenylindole (DAPI) (1:50, Harvey, USA). Images of murine specimens were visualized and captured with a fluorescence microscope (Olympus, Japan) using matching software, whereas panoramic images of tissue microarrays were acquired with the Panoramic MIDI Scanner (3DHISTECH LTD., Hungary).

TUNEL assays

Apoptosis was evaluated with a FragEL DNA fragmentation detection kit with a colorimetric TdT enzyme (Merck Millipore, Germany) following the manufacturer's protocol. Briefly, paraffin-embedded tissue samples were deparaffinized and subjected to permeabilization with 20 μg/ml proteinase K diluted in 10 mM Tris (pH 8.0) at RT for 20 min. The specimens were then treated to inactivate endogenous peroxidases by incubation with 3% H_2O_2 for 5 min at RT, and were subsequently equilibrated and labeled with terminal deoxynucleotidyl transferase for 1.5 h at 37 °C. After termination of the labeling reaction with Stop Solution (0.5 M EDTA, pH 8.0), nonspecific binding was blocked with blocking buffer (4% BSA in PBS) at RT for 10 min. Next, the incorporated TdT was detected by applying the peroxidase–streptavidin conjugate to the specimens for 30 min at RT, followed by application of a DAB solution (one tablet of DAB and one tablet of H_2O_2/urea in 1 ml of H_2O) onto the specimens for 10–15 min at RT. The slides were rinsed with double-distilled H_2O and counterstained with methyl green at RT for 3 min. After washing in ethanol and xylene, each specimen was mounted with resin and a coverslip. Evaluation under light microscopy (Olympus, Japan) was performed in a "blinded" fashion.

Ex vivo cytotoxicity assay

CD8$^+$ T cells were isolated from mouse spleens with the Mouse CD8$^+$ T-cell Isolation Kit (STEMCELL Technology Inc., Canada) according to the manufacturer's instructions. In vitro stimulation was performed with plate-bound stimulatory anti-CD3 and anti-CD28 antibodies (2 μg/ml each, BD Bioscience, USA). During 40 h of in vitro stimulation, T cells were cultured in RPMI 1640 medium supplemented with 10% FBS, rhIL-2 (100 U/ml, Pepro Tech Inc., USA), 2 mM L-glutamine, 1 mM sodium pyruvate, 0.1 mM non-essential amino acids, and 50 μM 2-mercaptoethanol in a humidified 37 °C incubator with 5% CO_2. Next, the effector cells were incubated with an anti-CD3 (10 μg/ml, BioLegend, USA) antibody for 30 min and then cocultured with CFSE-labeled P815 target cells at an E/T ratio of 10:1 for 2 h in 96-well round-bottom plates in a humidified 37 °C incubator. After the coculture period, the cells were stained with APC-Annexin V (2 μg/ml, BioLegend, USA). During flow-cytometric analysis, P815 target cells (CFSE$^+$ events) were gated, and the percentage of Annexin V$^+$ target cells was determined with the following formula: cytotoxicity (%) = target cell apoptosis% in effector-target cell mix − target cell spontaneous apoptosis%.

Adoptive transfer assay

CD147$^{+/+}$ or CD147$^{-/-}$ CD8$^+$ T cells were isolated from the spleen of CD45.1$^+$ wild-type mice or CD45.2$^+$ Bsg$^{\triangle T}$ mice, as described above. The isolated CD8$^+$ T cells were resuspended in PBS at 10^7 cells/ml. A total of 1×10^6 CD147$^{+/+}$ CD8$^+$ T cells and the same amount of CD147$^{-/-}$ CD8$^+$ T cells were mixed and intravenously transferred into 7- to 8-week-old male RAG mice that had been subcutaneously inoculated with 3×10^5 B16–F10 cells 1 day before. The recipient RAG mice were sacrificed 15 days after B16–F10 cell inoculation, and TILs were analyzed as described above.

Retroviral transduction of CD8$^+$ T cells

Murine *Runx3*-specific shRNA-encoding retroviruses, murine *Tbx21*-specific shRNA-encoding retroviruses, or negative control retroviruses were produced by Hanbio Biotechnology Co., Ltd. (Shanghai, China). The following shRNA hairpin sequences were used to interfere with *Runx3* or *Tbx21*:

Runx3-specific shRNA, 5′-TGCTGTTGACAGTGAGCGACAGGTT-CAACGACCTTCGATTT-AGTGAAGCCACAGATGTAAATCGAAGGTCGT TGAACCTGGTGCCTACTGCCTCGGA-3′, and

Tbx21-specific shRNA, 5′-TGCTGTTGACAGTGAGCGCCCTTCA-CATTCAGAAAGCAGA-TAGTGAAGCCACAGATGTATCTGCTTTCTGAA TGTGAAGGATGCCTACTGCCTCGGA-3′.

Retroviral transduction was performed as previously described.[53] Briefly, the cell concentration of activated CD8$^+$ T cells was adjusted to $1–3 \times 10^6$ cells/ml by adding an appropriate volume of T-cell stimulation medium. Retroviral supernatants (250 μL per well) were prepared in a 24-well plate supplemented with 10–16 μg/ml polybrene. Then, 250 μL of CD8$^+$ T-cell suspension was spin-transduced with 250 μL of retroviral supernatants in each well of a non-tissue-culture-treated 24-well plate at $2000 \times g$ for 90 min at 30 °C. After spin transduction, the plate was incubated in a 37 °C incubator with 5% CO_2 for at least 4 h (up to overnight or 12–16 h), and then the retroviral medium was replaced with T-cell culture medium containing IL-2 and incubated for another 36–40 h. After the incubation, the CD8$^+$ T cells were harvested, and knockdown of Runx3 or T-bet expression was confirmed by flow cytometry.

RNA isolation and qPCR

The total RNA was isolated from cells using the Total RNA Kit I (Omega Bio-tek, USA) according to the manufacturer's instructions. cDNA was reverse-transcribed from total RNA using a PrimeScript RT reagent kit (Takara Bio, Japan). A SYBR Green-based (Takara Bio, Japan) real-time PCR method was used to quantify the relative expression of mRNAs with the CFX 384 System (Bio-Rad, USA).

The primer sequences used were as follows: Ifng, 5′-GGATGC ATTCATGAGTATTGC-3′ and 5′-CCTTTTCCGCTTCCTGAGG-3′; Il12b, 5′-TGGTTTGCCATCGTTTTGCTG-3′ and 5′-ACAGGTGAGGTTCAC-T GTTTCT-3′; Ifit1, 5′-CTGAGATGTCACTTCACATGGAA-3′ and 5′-GTG CAT-CCCCAATGGGTTCT-3′; Ifit2, 5′-AGTACAACGAGTAAGGAGT-CACT-3′ and 5′-AGGCCAGTATGTTGCACATGG-3′; CXCL9, 5′-GGAGT TCGAGGAACCCTAG-TG-3′ and 5′-GGGATTTGTAGTGGATCGTGC-3′; CXCL10, 5′-TCAAGCCATGGT-CCTGAGACAA-3′ and 5′-CGCACCTCC ACATAGCTTACAG-3′; Runx3, 5′-CAGGTTCAACGACCTTCGATT-3′ and 5′-GTGGTAGGTAGCCACTTGGG-3′; Tbx21, 5′-AGCAAGGACGG CGAATGTT-3′ and 5′-GGGTGGACATATAAGCGGTTC-3′. All samples were normalized using β-actin as the internal control, which was detected with the primer sequences 5′-GGCTGTATTCCCCTCCA TCG-3′ and 5′-CCAGTTGGTAACAATGCCATGT-3′.

Tissue microarray (TMA) analysis and the NSCLC patient cohort

TMAs were purchased from Shanghai Biochip Company (China). The paraffin-embedded primary tumor samples were from 94 adenocarcinoma (ADC) patients and 75 squamous cell carcinoma (SCC) patients who underwent surgical resection between 2004 and 2011, and 52 of the samples were excluded from the study owing to serious tumor necrosis or the absence of TNM-stage information. The final study cohort consisted of 117 tumor samples (52 ADC and 65 SCC). The clinical characteristics of the patients are summarized in Table 1.

TMA immunofluorescence evaluation and quantitation

The density of CD8$^+$ TIL infiltration was calculated by dividing the counts of CD8$^+$ cells present in the desired compartment by the total area of the compartment defined by the software Case Viewer (3DHISTECH Ltd., Hungary).

The scores for the relative MFI of CD147 expression on CD8$^+$ TILs were determined using methods and algorithms described previously.[54] Briefly, quantification of the CD147 signal on CD8$^+$ cells within a desired tissue compartment was calculated by

dividing the total signal of CD147 intensity on positive CD8$^+$ cells by the number of CD8$^+$ cells in the area.

Statistical analysis

All tests for murine experiments were performed using GraphPad Prism software (La Jolla, CA). All data are presented as the mean ± standard deviation (STD), unless otherwise noted. Similar to a previous study,[34] two-sided paired Student's *t* tests were run on comparisons between Bsg$^{\triangle T}$ mice and Bsg^{WT} littermates and those between tumor-infiltrating and splenic cells from the same individual mouse, and unpaired *t* tests were used to compare two groups, while Dunn's test or one-way ANOVA was performed for multiple comparisons. *P* values <0.05 were considered statistically significant.

For the NSCLC patient cohort, all the statistical analyses were performed using SPSS 19.0 (SPSS, Inc., Chicago, IL, USA). The Mann–Whitney test was used to compare the distributions of the frequencies of CD8$^+$ TIL subsets between different groups defined by major clinical variants. Linear regression and correlation functions were used to assess the correlation between the density of CD8$^+$ TILs and the relative MFI of CD147 expression on CD8$^+$ TILs. Spearman correlation analysis was used to define the relationship between the frequency of CD147^{high} CD8$^+$ TILs within tumor islets and histological grade. Overall survival was defined as the time from diagnosis to death or the date of the last follow-up. Kaplan–Meier estimates and the log-rank test were used to compare OS between the group with a high (>24.64%) frequency of CD147$^+$ CD8$^+$ TILs and the group with a low frequency (≤24.64%), and between the group with a high density of CD8$^+$ TILs (>22.60) and the group with a low density (≤22.60). *P* values <0.05 were considered statistically significant.

ACKNOWLEDGEMENTS

The authors thank Xiwen Dong, Lijuan Wang, Qian He, and Xiaomin Li for their technical assistance and Jingmin Yu for assisting with mouse genotyping. This work was supported by grants from the National Natural Science Foundation of China (81572802), the National Basic Research Program of China (2015CB553700), and the Fourth Military Medical University Foundation for Development of Science and Technology (2019XB005).

AUTHOR CONTRIBUTIONS

Y.C., J.X., X.W., H.Y., Z.Y., W.W., P.W., T.G., Y.L., X.Y., and H.L. conducted the experiments and data analysis; J.X. and Z.-N.C. conceived the study and designed the experiments; Y.C., J.X., H.B., and Z.-N.C. discussed and interpreted the data; Y.C. and J.X. wrote the paper. All authors read and approved the final paper.

ADDITIONAL INFORMATION

The online version of this article (https://doi.org/10.1038/s41423-020-00570-y) contains supplementary material.

Competing interests: The authors declare no competing interests.

REFERENCES

1. Martinez-Lostao, L., Anel, A. & Pardo, J. How do cytotoxic lymphocytes kill cancer cells? *Clin. Cancer Res.* **21**, 5047–5056 (2015).
2. Thommen, D. S. & Schumacher, T. N. T cell dysfunction in cancer. *Cancer Cell* **33**, 547–562 (2018).
3. Li, H. et al. Dysfunctional CD8 T cells form a proliferative, dynamically regulated compartment within human melanoma. *Cell* **176**, 775–789 (2019).
4. Gubin, M. M. et al. High-dimensional analysis delineates myeloid and lymphoid compartment remodeling during successful immune-checkpoint cancer therapy. *Cell* **175**, 1014–1030 (2018).
5. Chew, V. et al. Delineation of an immunosuppressive gradient in hepatocellular carcinoma using high-dimensional proteomic and transcriptomic analyses. *Proc. Natl Acad. Sci. USA* **114**, E5900–E5909 (2017).
6. Khan, O. et al. TOX transcriptionally and epigenetically programs CD8(+) T cell exhaustion. *Nature* **571**, 211–218 (2019).
7. Wang, J. et al. Fibrinogen-like protein 1 is a major immune inhibitory ligand of LAG-3. *Cell* **176**, 334–347 (2019).
8. Li, J. et al. Co-inhibitory molecule B7 superfamily member 1 expressed by tumor-infiltrating myeloid cells induces dysfunction of anti-tumor CD8(+) T cells. *Immunity* **48**, 773–786 (2018).
9. Sun, C., Mezzadra, R. & Schumacher, T. N. Regulation and function of the PD-L1 checkpoint. *Immunity* **48**, 434–452 (2018).
10. Pal, S. K. et al. Clinical cancer advances 2019: annual report on progress against cancer from the American Society of Clinical Oncology. *J. Clin. Oncol.* **37**, 834–849 (2019).
11. Hashimoto, M. et al. CD8 T cell exhaustion in chronic infection and cancer: opportunities for interventions. *Annu. Rev. Med.* **69**, 301–318 (2018).
12. Ribas, A. & Wolchok, J. D. Cancer immunotherapy using checkpoint blockade. *Science* **359**, 1350–1355 (2018).
13. Sharma, P., Hu-Lieskovan, S., Wargo, J. A. & Ribas, A. Primary, adaptive, and acquired resistance to cancer immunotherapy. *Cell* **168**, 707–723 (2017).
14. Wei, S. C. et al. Distinct cellular mechanisms underlie Anti-CTLA-4 and anti-PD-1 checkpoint blockade. *Cell* **170**, 1120–1133 (2017).
15. Li, J., Ni, L. & Dong, C. Immune checkpoint receptors in cancer: redundant by design? *Curr. Opin. Immunol.* **45**, 37–42 (2017).
16. Koch, C. et al. T cell activation-associated epitopes of CD147 in regulation of the T cell response, and their definition by antibody affinity and antigen density. *Int. Immunol.* **11**, 777–786 (1999).
17. Weidle, U. H., Scheuer, W., Eggle, D., Klostermann, S. & Stockinger, H. Cancer-related issues of CD147. *Cancer Genomics Proteom.* **7**, 157–169 (2010).
18. Solstad, T. et al. CD147 (Basigin/Emmprin) identifies FoxP3+CD45RO+CTLA4+ -activated human regulatory T cells. *Blood* **118**, 5141–5151 (2011).
19. Landskron, J. & Tasken, K. CD147 in regulatory T cells. *Cell. Immunol.* **282**, 17–20 (2013).
20. Renno, T. et al. A role for CD147 in thymic development. *J. Immunol.* **168**, 4946–4950 (2002).
21. Arora, K. et al. Extracellular cyclophilins contribute to the regulation of inflammatory responses. *J. Immunol.* **175**, 517–522 (2005).
22. Gwinn, W. M. et al. Novel approach to inhibit asthma-mediated lung inflammation using anti-CD147 intervention. *J. Immunol.* **177**, 4870–4879 (2006).
23. Damsker, J. M. et al. Targeting the chemotactic function of CD147 reduces collagen-induced arthritis. *Immunology* **126**, 55–62 (2009).
24. Agrawal, S. M., Silva, C., Wang, J., Tong, J. P. & Yong, V. W. A novel anti-EMMPRIN function-blocking antibody reduces T cell proliferation and neurotoxicity: relevance to multiple sclerosis. *J. Neuroinflammation.* **9**, 64 (2012).
25. Nabeshima, K. et al. Emmprin, a cell surface inducer of matrix metalloproteinases (MMPs), is expressed in T-cell lymphomas. *J. Pathol.* **202**, 341–351 (2004).
26. Chen, X. et al. Inhibition of CD147 gene expression via RNA interference reduces tumor cell proliferation, activation, adhesion, and migration activity in the human Jurkat T-lymphoma cell line. *Cancer Investig.* **26**, 689–697 (2008).
27. Agrawal, S. M. et al. Extracellular matrix metalloproteinase inducer shows active perivascular cuffs in multiple sclerosis. *Brain* **136**, 1760–1777 (2013).
28. Guo, N. et al. CD147 and CD98 complex-mediated homotypic aggregation attenuates the CypA-induced chemotactic effect on Jurkat T cells. *Mol. Immunol.* **63**, 253–263 (2015).
29. Staffler, G. et al. Selective inhibition of T cell activation via CD147 through novel modulation of lipid rafts. *J. Immunol.* **171**, 1707–1714 (2003).
30. Hu, J. et al. Involvement of HAb18G/CD147 in T cell activation and immunological synapse formation. *J. Cell Mol. Med.* **14**, 2132–2143 (2010).
31. Ruiz, S., Castro-Castro, A. & Bustelo, X. R. CD147 inhibits the nuclear factor of activated T-cells by impairing Vav1 and Rac1 downstream signaling. *J. Biol. Chem.* **283**, 5554–5566 (2008).
32. Supper, V. et al. Association of CD147 and calcium exporter PMCA4 uncouples IL-2 expression from early TCR signaling. *J. Immunol.* **196**, 1387–1399 (2016).
33. Yao, H. et al. Important functional roles of basigin in thymocyte development and T cell activation. *Int. J. Biol. Sci.* **10**, 43–52 (2013).
34. Miller, B. C. et al. Subsets of exhausted CD8(+) T cells differentially mediate tumor control and respond to checkpoint blockade. *Nat. Immunol.* **20**, 326–336 (2019).
35. Sade-Feldman, M. et al. Defining T cell states associated with response to checkpoint immunotherapy in melanoma. *Cell* **175**, 998–1013 (2018).
36. Thommen, D. S. et al. A transcriptionally and functionally distinct PD-1(+) CD8(+) T cell pool with predictive potential in non-small-cell lung cancer treated with PD-1 blockade. *Nat. Med.* **24**, 994–1004 (2018).
37. Singer, M. et al. A distinct gene module for dysfunction uncoupled from activation in tumor-infiltrating T cells. *Cell* **166**, 1500–1511 (2016).
38. Cruz-Guilloty, F. et al. Runx3 and T-box proteins cooperate to establish the transcriptional program of effector CTLs. *J. Exp. Med.* **206**, 51–59 (2009).

39. Milner, J. J. et al. Runx3 programs CD8(+) T cell residency in non-lymphoid tissues and tumours. *Nature* **552**, 253–257 (2017).
40. Hahn, J. N., Kaushik, D. K. & Yong, V. W. The role of EMMPRIN in T cell biology and immunological diseases. *J. Leukoc. Biol.* **98**, 33–48 (2015).
41. Zhu, X., Song, Z., Zhang, S., Nanda, A. & Li, G. CD147: a novel modulator of inflammatory and immune disorders. *Curr. Med. Chem.* **21**, 2138–2145 (2014).
42. Guo, N. et al. A critical epitope in CD147 facilitates memory CD4(+) T-cell hyperactivation in rheumatoid arthritis. *Cell. Mol. Immunol.* **16**, 568–579 (2019).
43. Geng, J. J. et al. Targeting CD147 for T to NK lineage reprogramming and tumor therapy. *EBioMedicine* **20**, 98–108 (2017).
44. Chen, R. et al. CD147 deficiency in T cells prevents thymic involution by inhibiting the EMT process in TECs in the presence of TGFbeta. *Cell. Mol. Immunol*. https://doi.org/10.1038/s41423-019-0353-7 (2020).
45. Carow, B. et al. lck-driven Cre expression alters T cell development in the thymus and the frequencies and functions of peripheral T cell subsets. *J. Immunol.* **197**, 2261–2268 (2017).
46. Shan, Q. et al. The transcription factor Runx3 guards cytotoxic CD8(+) effector T cells against deviation towards follicular helper T cell lineage. *Nat. Immunol.* **18**, 931–939 (2017).
47. Ciucci, T., Vacchio, M. S. & Bosselut, R. A STAT3-dependent transcriptional circuitry inhibits cytotoxic gene expression in T cells. *Proc. Natl Acad. Sci. USA* **114**, 13236–13241 (2017).
48. Ganesan, A. P. et al. Tissue-resident memory features are linked to the magnitude of cytotoxic T cell responses in human lung cancer. *Nat. Immunol.* **18**, 940–950 (2017).
49. Nagarsheth, N., Wicha, M. S. & Zou, W. Chemokines in the cancer microenvironment and their relevance in cancer immunotherapy. *Nat. Rev. Immunol.* **17**, 559–572 (2017).
50. Sharpe, A. H. & Pauken, K. E. The diverse functions of the PD1 inhibitory pathway. *Nat. Rev. Immunol.* **18**, 153–167 (2018).
51. Chow, M. T. et al. Intratumoral activity of the CXCR3 chemokine system is required for the efficacy of anti-PD-1 therapy. *Immunity* **50**, 1498–1512 (2019).
52. Schalper, K. A. et al. Objective measurement and clinical significance of TILs in non-small cell lung cancer. *J. Natl. Cancer Inst*. **107**, dju435 (2015).
53. Kurachi, M. et al. Optimized retroviral transduction of mouse T cells for in vivo assessment of gene function. *Nat. Protoc.* **12**, 1980–1998 (2017).
54. Kluger, H. M. et al. PD-L1 studies across tumor types, its differential expression and predictive value in patients treated with immune checkpoint inhibitors. *Clin. Cancer Res.* **23**, 4270–4279 (2017).